ACS OMEGA

Open Access

http://pubs.acs.org/journal/acsodf

Article

Geochemistry and Origin of Deep and Ultradeep Crude Oils from the Jurassic Qigu Formation, Yongjin Area, Central Junggar Basin, NW China

Yansheng Qu, Jinqi Qiao,* Ningning Zhong, Wei Li, Guanlong Zhang, Hongzhou Yu, Gui Wang, and Fangchao Yan

Cite This: *ACS Omega* 2025, 10, 2735−2761

Read Online

ACCESS | Metrics & More | Article Recommendations

ABSTRACT: Recently, there has been an increasing focus on deep and ultradeep oil and gas exploration and development. The Upper Jurassic Qigu Formation (Fm.) in the Yongjin region, located in the central area of the petroleum-bearing Junggar Basin, develops typically deep and ultradeep hydrocarbon reservoirs, but there is currently limited knowledge of the geochemical characteristics and origins of the oils in the reservoirs. A comprehensive analysis of the molecular characteristics and carbon isotopes of the oil and extractable organic matter (OM) samples from the Qigu reservoirs, as well as source rocks from the Middle Permian lower Wuerhe and Lower Permian Fengcheng Fm., was carried out to elucidate the thermal maturity, biological sources, and biodegradation scale of the OM, as well as the depositional environment of the related source rocks. The results suggest that the Qigu oils originated primarily from source rocks formed in a hypersaline lacustrine environment with paleoredox conditions of bottom water ranging from reducing to suboxic conditions. Furthermore, the biological sources of oils predominantly originated from bacteria, followed by algae. The degradation scales range between 3 and 4, and the thermal maturity is in the oil window for the samples examined. The OM of the Permian source rocks in the Yongjin region are in the high thermal maturity stage due to their ultradeep burial, thereby providing limited information to oil and source correlation. By combining more than 1000 published data from the entire basin, significant differences between the Jurassic and Permian source rocks, as well as minor differences between the lower Wuerhe (i.e., the ratios of Pr/*n*-C_{17} of <0.5, Ph/*n*-C_{18} of <0.5, Pr/Ph of >1.5, C_{27}/C_{29} sterane of >0.4, and hopanoids/steranes of >1 as well as the higher C_{20}/C_{23} Tri ratios) and Fengcheng source rocks (i.e., β-carotane/*n*-C_{max} ratios of >0.1 and some samples with C_{28} steranes concentrations of <10% in the normalized concentrations of C_{27}, C_{28}, and C_{29} steranes), were observed, and the origins of the oils were determined. The oil-source correlation suggests that the oils most likely originated from the lower Wuerhe Fm. without strictly excluding the possibility of a contribution from the Fengcheng Fm.

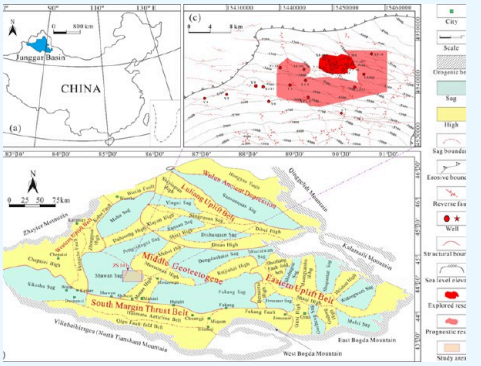

1. INTRODUCTION

In recent years, there has been an increasing investment in the exploration and development of deep (>4500 m) and ultradeep (>6000 m) oil and gas resources worldwide, which have become an important part of deep earth research.[1−4] The contribution of deep and ultradeep oil and gas resources to global oil production is also on the rise.[5,6] At present, the proven deep and ultradeep oil and gas resources in China have reached 67.1×10^9 tons of oil equivalent, accounting for 34% of the total oil and gas resources in China.[7] Deep and ultradeep oil and gas resources have become the main targets of major oil and gas discovery in China, and large-scale discoveries have been made in the deep layers of the Tarim, Sichuan, Junggar, Songliao, Yin'e and Bohai Bay Basin.[8−11] However, multiple sets of potential source rocks are generally developed in deep and ultradeep hydrocarbon systems and have undergone complex structural evolution. The different hydrocarbon generation processes from various source rocks and the multistage reservoir reconstructions contribute to the complexity of crude oil types in deep and ultradeep oil and gas systems, which significantly hinders the determination of the sources and formation mechanisms of crude oils.[12,13]

The Junggar Basin is a prototypical superimposed petroleum-bearing basin located in the northern region of the Xinjiang Uygur Autonomous Region in northwest China (Figure 1a). The origins of the Jurassic crude oils are currently unclear, and the Jurassic crude oils found in various regions of the basin are

Received: September 15, 2024
Revised: December 25, 2024
Accepted: December 26, 2024
Published: January 15, 2025

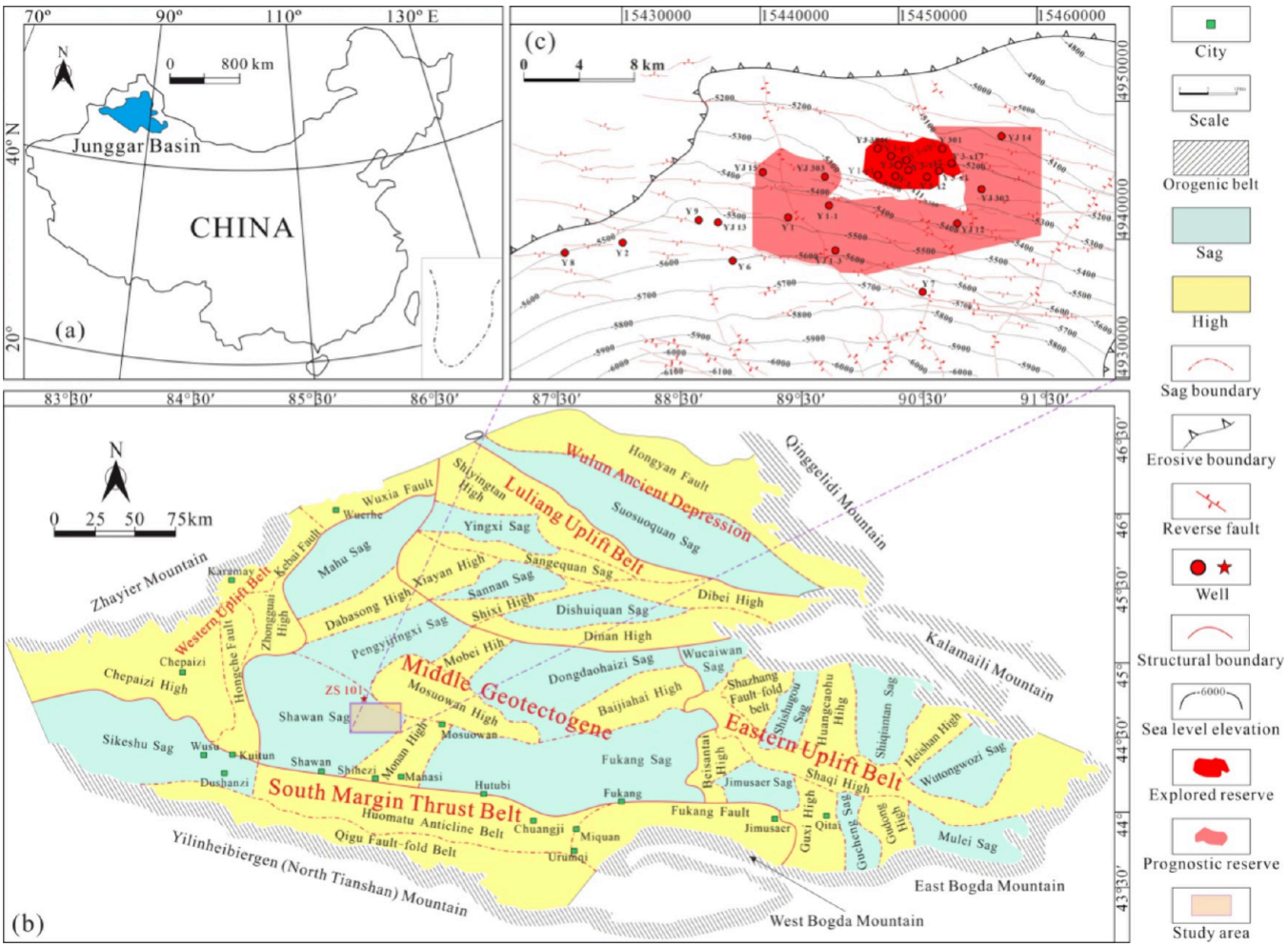

Figure 1. (a) Schematic map showing the location of the Junggar Basin in China, (b) its structure outline map, and (c) the study area and well locations. Note: (a) and (b) were modified with permission from reference.[18] Copyright [2022] [2022 ELSEVIER B.V.].

generated by source rocks from different strata. For example, the Jurassic crude oils found in the central Junggar Basin, the Cainan oilfield in the eastern Junggar Basin, and the slope zone of the Mahu Sag in the northwest Junggar Basin are primarily generated by the Lower Jurassic Badaowan Formation (Fm.) coal-bearing source rocks,[14] are mixed generated by the three sets of source rocks,[15] and are generated by the Lower Permian Fengcheng Fm.,[16] respectively. This ambiguity stems from the presence of multiple sets of source rocks under the main Jurassic hydrocarbon reservoirs (i.e., the Middle Jurassic Xishanyao and Upper Jurassic Qigu Fm.), which includes the Fengcheng Fm. and Middle Permian lower Wuerhe Fm. (the lower Wuerhe Fm. represents the isochronous stratigraphic unit of the Lucaogou and Pingdiquan Fm. in various areas of the basin), as well as the Badaowan Fm. (e.g., refs 16−19). Furthermore, it has been challenging to identify effective geochemical parameters to distinguish between the source rocks of the Fengcheng Fm. and the lower Wuerhe Fm. because they formed under very similar depositional environments and share very similar organic matter (OM) origins.[16−19] These similarities make it difficult to correlate oil and sources in the study area in detail. Furthermore, some molecular parameters exhibit convergent in the high and over high thermal maturity of OM, for example, the distribution patterns of *n*-alkanes of across diverse source rocks show abundant *n*-alkanes below *n*-C_{20} characterized by a lack of odd/even predominance, so it complicates the correlation between the oil and the source in deep and ultradeep reservoirs.

The Yongjin region encompasses an exploration area of approximately 1200 km^2 (Figure 1b). Positioned to the east of the Mosuowan High and Monan High as well as west of the Shawan Sag, this area holds significant potential for enhancing the hydrocarbon reservoirs in the western exploration area of the Shengli Oilfield, operated by Sinopec (China Petrochemical Corporation). The reported Jurassic cumulative prognostic reserves stand at nearly 83.6×10^6 tons. The Qigu Fm. reservoir, buried at a depth of 5500−6500 m, contains significant deep and ultradeep oil and gas resources potential, with over 62×10^6 tons of oil reserves (Figure 2). The Qigu Fm. is in unconformity contact with both the overlying Cretaceous Qingshuihe Fm. and the underlying Xishanyao Fm (Figure 2). The lithological association, which is mainly composed of sandy conglomerate in the bottom, sandstone and siltstone in the middle, and mudstone in the upper, is very conducive to the accumulation and preservation of oil and gas (Figure 2). Multiple sets of important source rocks, buried at depths of 8000−10,000 m, belong to ultradeep source rocks in the Shawan Sag. The discovery of industrial oil flows in the Y 1 well in 2004 prompted a significant increase in Sinopec's investment in exploration and development activities. As part of this endeavor, 34 development and evaluation wells targeting the Qigu Fm. have been strategically deployed up to 2024, with 24 of these wells drilled

https://doi.org/10.1021/acsomega.4c08477
ACS Omega 2025, 10, 2735−2761

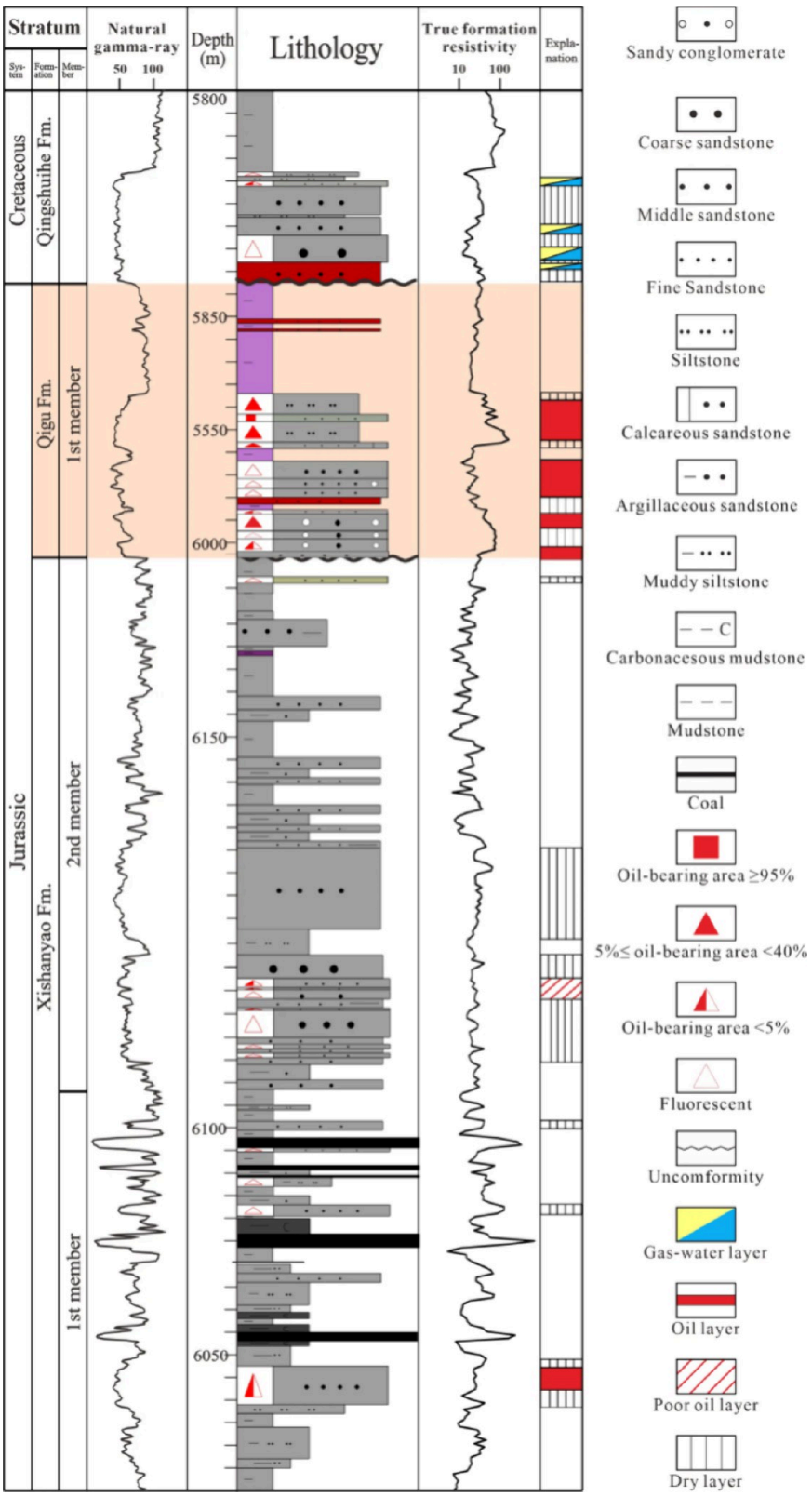

Figure 2. Comprehensive stratigraphic column diagram of the Yongjin area in the Junggar Basin, China.

into oil layers (Figure 1c). Following preliminary exploration, several of these development wells demonstrated significant production potential. Specifically, in the Y 1, Y 2, Y 3, Y 301, and YJ 303 wells, as well as some adjacent wells, substantial industrial oil flow has been achieved from the Qigu Fm., with a cumulative oil production of 90 tons and a cumulative gas production of 2.8 $\times$ 10^4 m^3 per day. The Y 3-x2 well initially recorded an oil production of 56 tons per day, and the Y 3-x12 well yielded 35.8 tons of oil per day. These findings strongly indicate the considerable promise of the Yongjin area, with ongoing

https://doi.org/10.1021/acsomega.4c08477
ACS Omega 2025, 10, 2735−2761

exploration and development efforts expected to yield further positive results. The preliminary exploration suggests that the Yongjin area possesses hydrocarbon accumulation features, such as multistage charging, high formation pressures, different hydrocarbon enrichment mechanisms, and reservoirs distinct from hydrocarbon source rocks. The current understanding of Qigu Fm. is limited due to the ambiguity regarding the origin of oils in the reservoirs. This study comprehensively interpreted the saturated and aromatic hydrocarbon data as well as the isotopic composition of the oil and extractable OM (EOM) samples from the Qigu Fm. in the Yongjin area and compared them to the molecular characteristics of the source rocks. The main objective is to offer a comprehensive understanding of the characteristics of the oils, thereby interpreting the origin of OM and the depositional environment of the related source rocks of the oils, as well as assessing the thermal maturity and biodegradation levels of the oils. These insights are essential for identifying the origins of the oils in the Yongjin area and contribute to an enhanced understanding of the geological processes involved in the formation and evolution of the oils in the Qigu reservoirs.

2. GEOLOGICAL SETTING

The Junggar Basin, which exhibits a triangular shape, spans over 700 km from east to west and 370 km from north to south, encompassing a total area of approximately 13×10^4 km^2, with an average elevation of approximately 500 m (Figure 1b).[18,20] The basin is flanked by several mountain ranges, including the Zhayier Mountain to the northwest, the Kalamaili Mountain and the Qinggelidi Mountain to the northeast, the Yilinheibiergen Mountain to the southwest, and the Bogda Mountain to the southeast (Figure 1b).

Geologically, the Junggar Basin lies within the central stable region of the Junggar-Tuha terrane and functions as the confluence zone of the plates of Siberian, Tarim, and Kazakhstan.[21] The basin has been subjected to a succession of tectonic events, including the Hercynian, Indochinese, Yanshan, and Himalayan movements, leading to the development of an intricate and diverse tectonic framework within the region.[22]

The basement of the Junggar Basin exhibits a complex dual-layer structure, which is the pre-Cambrian crystalline basement superimposed with the Hercynian fold mountain basement. Overlying the basement, sedimentary layers ranging from Carboniferous to Cretaceous are prevalent across most of the basin. In the Yongjin area, the sedimentary sequences extend to the Quaternary systems. The currently deepest well in the study area, the ZS 101 well, has reached down to the Fengcheng Fm. Around the ZS 101 well, the lithology of the Fengcheng Fm. is mainly composed of mudstone, dolomitic mudstone, and limestone mudstone with some argillaceous siltstone, while that of the lower Wuerhe Fm. contains a higher proportion of coarser components, e.g., sandstone and argillaceous sandstone (Figure 3). During the Late Carboniferous and early Middle Jurassic periods, the study area was situated in a negative tectonic unit. The structural development of the Chepaizi-Mosuowan area have undergone a reversal and gradual uplift during the Middle and Late Jurassic periods due to the Yanshan Movement, which ultimately led to the formation of the Mosuowan High. Located on the dipping slope, the Yongjin area benefits from the continuous southward dip of the structure and provides favorable structural conditions for the accumulation of oil and gas resources in the area. The structure of the Qigu Fm.

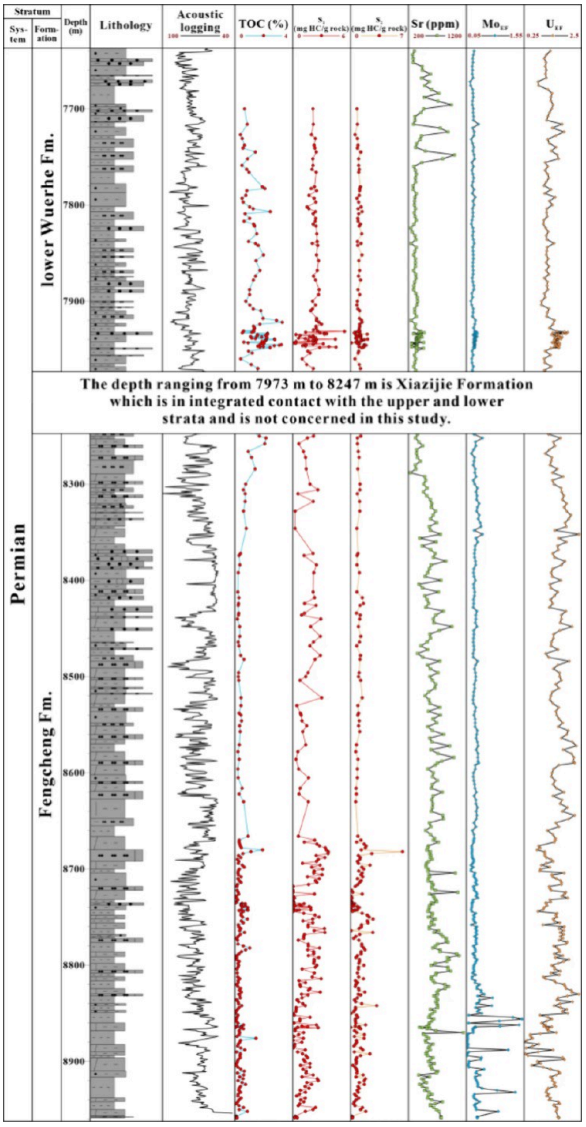

Figure 3. Stratigraphic distributions of lithology, TOC content, S_1 value, S_2 value, Sr concentration, Mo_{EF} and U_{EF} of the lower Wuerhe and Fengcheng Formation of the ZS 101 well in the Yongjin area in the Junggar Basin, China.

in the Yongjin area is relatively simple and is characterized by a broad and gently sloping structural background.

The study area experienced significant erosion effects, especially in the north and west, due to the multistage uplift of the Mosuowan High. The erosion mainly affected the areas around the Y 1 and Y 3 wells as well as the eastern region, forming a large-scale stratigraphic erosion trap. Consequently, only one member of the Qigu Fm. remains in the Yongjin area, with stratum thicknesses ranging between 40 and 60 m. This member consists mainly of purplish-red mudstone segments. The upper part consists of purplish-red mudstone interspersed with purplish-red and gray sandstone, while the lower part features gray sandstone interspersed with purplish-red mudstone (Figure 2).

3. SAMPLES AND METHODS

3.1. Samples and Preparation. A total of 76 samples were analyzed in this study. Among them, 14 samples are oil samples from the Y 1 well, Y 3 well, Y 9 well, Y 301 well, YJ 304C well, YJ

https://doi.org/10.1021/acsomega.4c08477
ACS Omega 2025, 10, 2735−2761

Table 1. Physical Parameters of the Oil Samples from the Qigu Formation in the Yongjin Area of the Junggar Basin, China[a]

sample type	well	depth (m)	density (20 °C)	viscosity (50 °C)	condensation point	wax precipitation point	wax content (%)	resin content (%)	asphaltene content (%)
Oil	Y 1−3	5969.00−5996.00	0.84	3.0	11	19.8	17.43	8.21	4.45
	Y 1	5873.40−5888.10	0.88	28.8	4	n.d.	16.43	n.d.	n.d.
	Y 2	6051.00−6061.60	0.84	4.0	8	n.d.	10.50	7.70	n.d.
	YJ 12	6159.20−6166.00	0.88	40.7	10	21.8	15.42	13.35	5.68
	Y 301	5541.60−5552.00	0.87	50.0	9	19.3	18.22	11.68	5.45
	Y 301	5541.60−5552.00	0.87	51.0	10	20.6	17.74	12.65	4.37
	Y 301	5541.60−5552.00	0.85	57.0	7	20.3	17.11	10.17	3.56
	Y 3-x1	5716.00−5724.00	0.91	327.5	9	n.d.	2.37	8.65	6.38
	Y 3-x2	5817.20−5829.00	0.87	21.0	9	18.9	17.98	9.87	5.26
	Y 3-x2	5817.20−5829.00	0.86	19.0	9	21.4	18.67	9.72	4.83
	Y 3-x11	6021.00−6033.00	0.86	13.0	9	20.9	17.67	10.57	4.52
	Y 3-x17	5714.20−5730.30	0.89	381.6	6	n.d.	12.95	13.48	5.64
	Y 3-p1	5894.00−6616.00	0.85	28.0	7	20.0	16.94	11.54	4.15
	Y 3-p1	5894.00−6616.00	0.86	9.0	8	20.1	17.15	10.87	4.38
	Y 3-cp1	5775.85−6110.80	0.85	11.7	7	20.4	16.63	11.32	4.69
	Y 3-cp1	5775.85−6110.80	0.86	13.0	7	18.5	16.21	11.48	4.83
	Y 3-cp1	5775.85−6110.80	0.86	18.0	12	21.2	16.85	10.78	4.57
	Y 3-cp1	5775.85−6110.80	0.86	15.0	8	19.7	16.78	10.93	4.16

[a]n.d., no detected.

302 well, Y 1-p1 well, Y 3-x11 well, Y 3-x12 well, and Y 3-cp1 well, as well as 49 samples are EOM samples from sandstone/reservoirs from the Y 1−1 well, YJ 1−3 well, Y 1 well, Y 2 well, Y 3 well, Y 6 well, Y 7 well, Y 8 well, YJ 12 well, YJ 14 well, YJ 15 well, Y 301 well, YJ 302 well, YJ 303 well, and Y 3-x17 well (Figure 1c). The source rocks were sampled from the ZS 101 well (5 source rocks from the lower Wuerhe Fm. and 8 from the Fengcheng Fm.). The TOC contents of the Fengcheng Fm. are mostly lower than 1.0%, while of the lower Wuerhe Fm., they are higher, ranging from 0.38 to 3.28% (average 1.46%) (Figure 3). S_1 (quantity of free and sorbed hydrocarbon, mg HC/g rock) values are similar between the Fengcheng Fm. and the lower Wuerhe Fm., while S_2 (generated hydrocarbon, mg HC/g rock) values are lower in the Fengcheng Fm. in comparison to those in the lower Wuerhe Fm (Figure 3). Moreover, the Sr (strontium) concentrations indicate that both the Fengcheng Fm. and the lower Wuerhe Fm. were deposited under hypersaline and saline conditions, and the paleosalinity decreased from the Fengcheng Fm. to the lower Wuerhe Fm. (Figure 3). Additionally, the oxygen contents in the water column of the Wuerhe Fm. were higher than that of the Fengcheng Fm., which is supported by the higher U (uranium)$_{EF}$ and Mo (monium)$_{EF}$ contents in the Fengcheng Fm. (Figure 3). Among the source rocks, four samples taken from depths of 7941.00 and 7955.40 m in the lower Wuerhe Fm., as well as from 8737.00 and 8742.50 m in the Fengcheng Fm. were used to make polished sections for organic petrography analysis.

The densities (at 20 °C; 0.1 MPa) and viscosities (at 50 °C; 0.1 MPa) of the oils range from 0.84 to 0.91 g/cm^3 (avg. 0.86 g/cm^3) and from 3.0 to 381.6 mPa s (52.23 mPa s), respectively. The condensation points are 4−12 °C (8.4 °C on average), and wax precipitation points are 18.2−21.8 °C (20.07 °C on average), respectively (Table 1). Moreover, the contents of wax, resin, and asphaltene are 2.37−18.67%, 7.70−13.48%, and 3.56−6.38%, respectively (Table 1).

In the present study, an accelerated solvent extraction (ASE) was employed to extract OM from the sandstones and source rocks. Powdered samples, weighing 80−120 g and sized <80 mesh, were extracted using dichloromethane (DCM). Post-extraction, elemental sulfur was removed by adding copper powder to the oils and extracts.

The oils and EOM samples were subjected to fractionation and separated into four fractions: aliphatic hydrocarbons, aromatic hydrocarbons, NSO (nitrogen-, sulfur-, and oxygen-containing) components, and asphaltenes, wherein the asphaltene fraction was precipitated via a settlement of extracts and oils dissolved in *n*-hexane for a duration exceeding 12 h. The remaining three fractions were subjected to washing with eluents of different polarities, including *n*-hexane (30 mL), a mixed solvent of *n*-hexane/DCM (20 mL), and anhydrous ethanol (10 mL), followed by trichloromethane (10 mL) in turn via column chromatography.

The separated saturated hydrocarbon and aromatic components were volatilized to dryness at temperatures below 40 °C, while the NSO and asphaltene components were volatilized to dryness at temperatures not exceeding 60 °C. Following the desiccation process, approximately 30 μg of each sample was weighed and then deposited into appropriate tin cups or tin bags. Subsequently, the tin cups or tin bags containing the samples were folded or wrapped into a compact shape using a clamp and then positioned on a sample plate to determine the stable organic carbon isotope composition (δ^{13}C).

3.2. Analysis Methods. A Leica DM4500P microscope was used to identify maceral composition and measure the vitrinite reflectance (VR_r). A standard sample with a known reflectance (Yttrium−Aluminum-Garnet, 1.725%) was used to calibrate the microscope before each measurement. See literature[17−19,23] for more information related to the process of the analysis.

The aliphatic and aromatic hydrocarbon fractions were subjected to gas chromatography (GC)-mass spectrometry (MS) analysis using an Agilent 6890 gas chromatograph coupled to a 5975i mass spectrometer and an Agilent 7890B gas chromatograph coupled to a 5977A mass spectrometer, respectively. The equipment operational settings and temperature programs were comprehensively described in detail in the work of refs 18,20. The molecular parameter quantification was based on evaluating the peak areas of specific ion chromatograms, with the compound identification achieved through

https://doi.org/10.1021/acsomega.4c08477
ACS Omega 2025, 10, 2735−2761

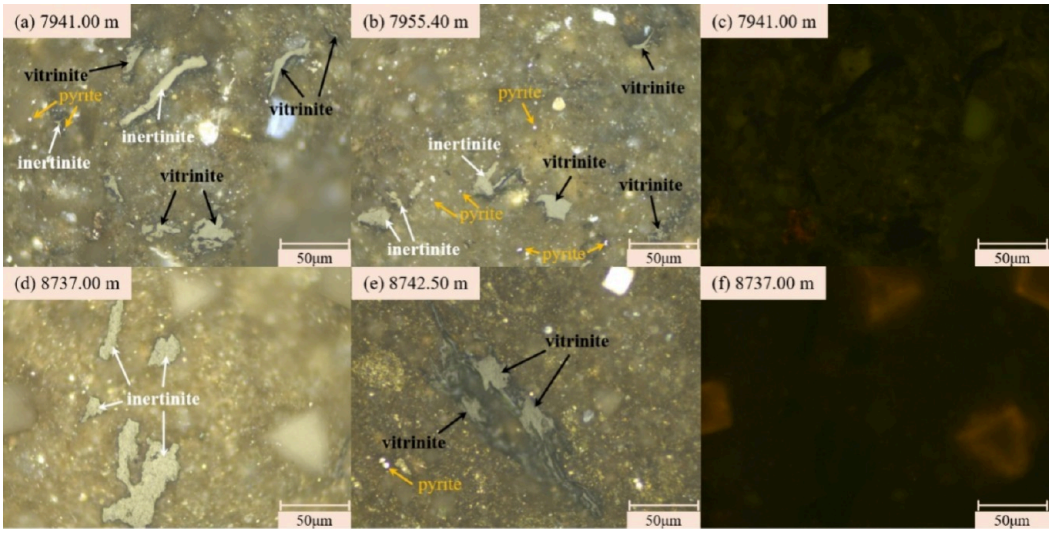

Figure 4. Photomicrographs representative of the macerals and pyrite under (a−e) incident white light and (c−f) fluorescence mode in the source rocks from the lower Wuerhe Formation (a−c) and Fengcheng Formation (d−f) in the ZS 101 well located in the Yongjin area in the central Junggar Basin, China.

meticulous comparison of the elution sequences with published literature (e.g., refs 17,24,25).

The analysis of $\delta^{13}C$ was determined by using a FLASH HT EA-MAT 253 isotope ratio mass spectrometer (IRMS). High-purity helium gas (99.999%) served as the carrier maintaining a flow rate of 100 mL/min and a backflush flow of 250 mL/min. High-purity oxygen gas (99.995%) was used as the combustion gas at a flow rate of 250 mL/min. The reactor temperature was 980 °C, and the filling materials of the reaction furnace are chromium oxide, copper, and silver−containing cobalt oxide. The USGS-61 (δ^{13}CPDB: −35.05 ± 0.04‰), USGS-62 (δ^{13}CPDB: −14.79 ± 0.04‰), and USGS-63 (δ^{13}CPDB: −1.17 ± 0.04‰) were used as standard materials. In order to make sure the accuracy and precision of the analysis, the standard samples were regularly analyzed before and after the measurement, and each sample was analyzed three times to ensure reproducibility of the results.

All analyses were performed at the State Key Laboratory of Petroleum Resources and Engineering, China University of Petroleum (Beijing).

4. RESULTS

4.1. Organic Petrography. Vitrinite is the predominant macerals (Figure 4a,b,e) with some inertinite macerals (Figure 4a,b,d). The VR_r values range from 1.79% (7941.00 m of the lower Wuerhe Fm.) to 1.95% (8742.50 m of the Fengcheng Fm.) with an average value of 1.86%, indicating a high thermal maturity stage. Due to the high thermal maturity of the OM, liptinite macerals are hard to observe (Figure 4c,f). Pyrites are abundant in all samples occurring as euhedral crystals in most cases (Figure 4a,b,e).

4.2. Molecular Composition. *4.2.1. n-Alkanes, Acyclic Isoprenoids, and Bicyclic Alkanes.* The total ion chromatogram (TIC) chromatograms of the studied oil and EOM samples reveal that the primary compounds are normal alkanes (*n*-alkanes) in the range from *n*-C_{14} to *n*-C_{31} with an unimodal distribution exhibiting maxima at *n*-C_{18} or *n*-C_{19} in most samples (Figure 5a,b; Table 2). The CPI and the OEP values are 0.90−1.13 and 0.96−1.15, respectively (Table 2). Additionally, the TAR (terrigenous/aquatic ratio) and P_{aq} (submerged/floating macrophytes) range from 0 to 2.77 (0.32 on average) and from 0.68 to 0.98 (0.82 on average), respectively (Figure 5a,b) (Table 2).

Moreover, the presence of isoprenoids, such as *i*-C_{15} (farnesane), *i*-C_{16}, pristane (Pr), phytane (Ph), *i*-C_{25} (PMI), and *i*-C_{30} (squalane), is evident (Figure 5a,b). Relative concentration analyses reveal values for Pr and Ph in comparison to their adjoining *n*-alkanes (i.e., Pr/*n*-C_{17} and Ph/*n*-C_{18}) of 0.24−1.08 and 0.18−2.00, respectively. Furthermore, the Pr/Ph ratios exhibit a range between 0.19 and 1.92 (Table 2). Notably, significant variations in β-carotane abundances (m/z 125) are observed, with β-carotane/*n*-C_{max} ratios spanning from 0 to 0.42 (averaging 0.07) (Table 2). Short-chain monomethylalkanes (MMAs) are also abundant for the samples examined (Figure 5a,b).

The chromatograms of the source rocks show that the primary compounds are *n*-alkanes in the range from *n*-C_{14} to *n*-C_{20} with an unimodal distribution (Figure 6a,b; Table 3). The isoprenoids, such as *i*-C_{16}, Pr, and Ph, are abundant (Figure 6a,b). Pr/*n*-C_{17} and Ph/*n*-C_{18} are 0.30−0.71 and 0.62−1.11, respectively, and the Pr/Ph ratios are 0.42−1.35 (Table 3). Moreover, β-carotane is hard to observe (Table 3). The MMAs concentrations are also high for the source rocks (Figure 6a,b).

4.2.2. Terpanes. In the mass chromatogram at m/z 191, terpanes are observed. Tricyclic terpanes (Tri) ranging between C_{19} and C_{29}, excluding C_{27}, are present in all oil and EOM samples (Figure 5c,d). Within the short chains of Tris, trends include increasing concentrations from C_{19} to C_{21} Tri and decreasing concentrations from C_{23} to C_{25} Tri with C_{24}/C_{23} Tri ranging from 0.36 to 0.58 and $C_{19}/(C_{19} + C_{23})$ Tri from 0.10 to 0.67, respectively (Figure 5c,d; Table 4). Furthermore, the concentrations of C_{22} Tri are lower than those of C_{21} or C_{23} Tri with C_{22}/C_{21} Tri ratios ranging between 0.15 and 0.27 (Figure 5c,d; Table 4). The concentrations of C_{25} Tri are generally higher than those of C_{26} Tri, with C_{26}/C_{25} Tri ratios being in the range of 0.90 to 1.73. The extended Tri ratio (ETR), calculated as (C_{28} Tris + C_{29} Tris)/Ts, ranges between 0.80 and 2.92. C_{24} tetracyclic terpane (Tet) is observed in all samples with C_{24} Tet/C_{23} Tri ranging from 0.12 to 0.49 (Figure 5c,d; Table 4).

https://doi.org/10.1021/acsomega.4c08477
ACS Omega 2025, 10, 2735−2761

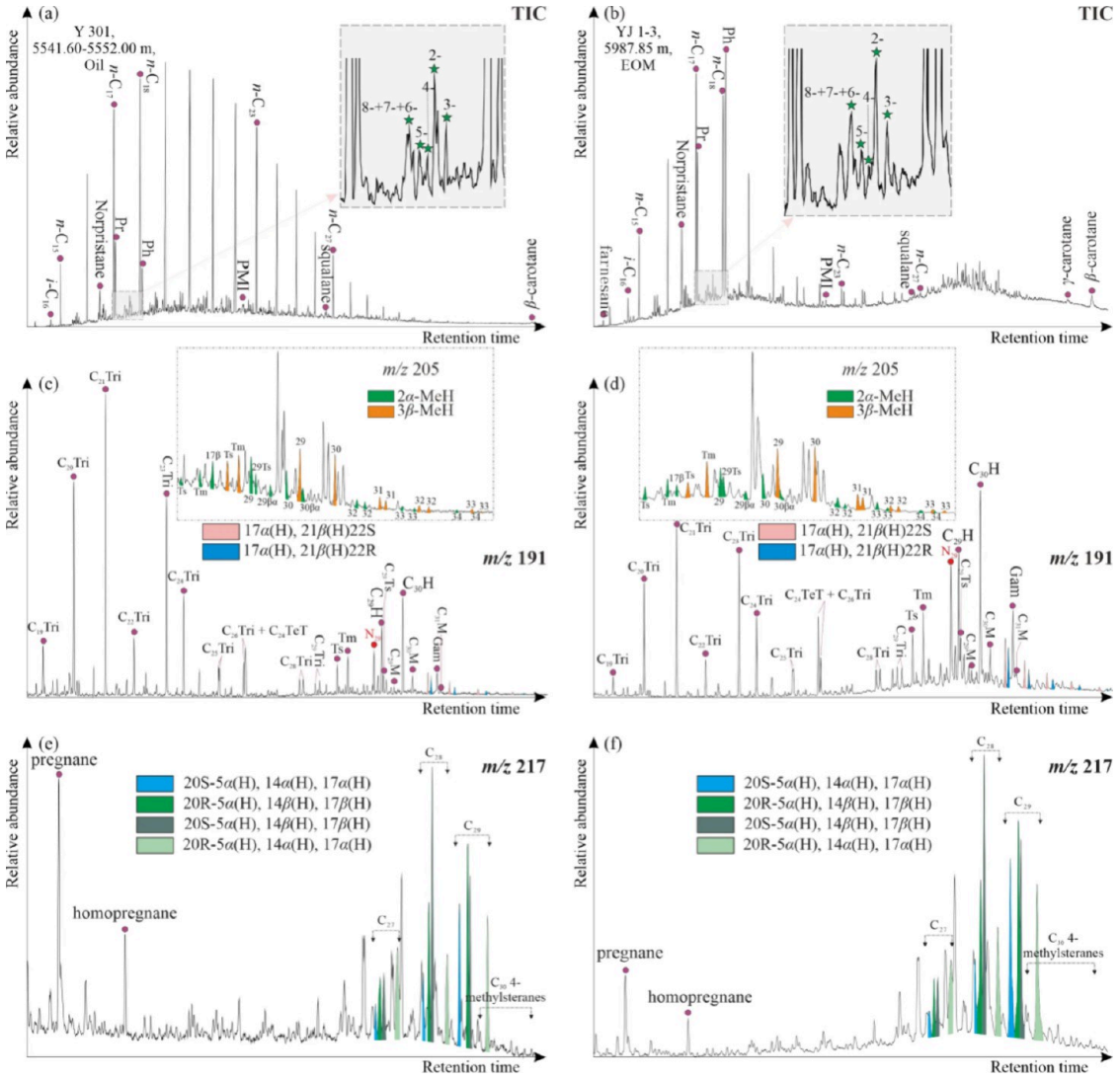

Figure 5. Distribution of partial mass chromatograms of the aliphatic fraction in representative samples (figures on the left represent the oil sample from the Y 301 well and those on the right represent the EOM sample from the YJ 1−3 well). (a, b) Total ion chromatogram (TIC), (c, d) mass chromatograms showing the distributions of hopanes (m/z 191) and methylhopanoids (m/z 205), as well as (e, f) mass chromatograms showing the distributions of steranes (m/z 217).

A series of hopanes (Hop) were detected in the studied samples, spanning from C_{27} to C_{35} except for C_{28} and pecking at C_{30} in most cases (as indicated by C_{29}/C_{30} Hop ratios of 0.40−1.15 with an average value of 0.71) (Figure 5c,d; Table 4). Furthermore, C_{31-35} Hop encompasses multiple stereoisomers with C_{31} and C_{32} Hop 22S/(22S + 22R) being 0.48−0.62 and 0.54−0.65, respectively (Figure 5c,d; Table 4). Moreover. Ts/(Ts + Tm) ratios range from 0.23 to 0.60, and C_{31} 22R/C_{30} Hop ratios range from 0.14 to 0.36, respectively (Table 4). Gammacerane (Gamm) shows high concentrations with a Gamm/C_{30} Hop ratio ranging between 0.14 and 1.04 (Figure 5c,d; Table 4).

Moreover, it is noteworthy that two series of methylhopanoids (MeH) (m/z 205) including 2α-MeH and 3β-MeH as well as C_{29} 25-norhopane (C_{29}NH) are abundant in the oils and EOM samples with C_{29}NH/C_{30} Hop ratios of 0.00−0.23 (Figure 5c,d; Table 4).

The distributions of terpanes of the source rocks are characterized by the highest concentrations of C_{30} Hop (Figure 6c,d) and the used parameters related to terpanes are listed in Table 3.

4.2.3. Steroids. Steroids for the studied oil and EOM samples are identified by monitoring m/z 217 ion chromatograms (Figure 5e,f), which shows that C_{29} steranes (34.44−54.95%) and C_{28} steranes (25.71−43.92%) are predominant, while C_{27} steranes (11.18−28.21%) are relatively minor in most cases (Figure 5e,f) (Table 4). The C_{29} $\alpha\alpha\alpha$ 20S/(20S + 20R) and $\beta\beta$/($\beta\beta$ + $\alpha\alpha$) steranes ratios range from 0.42 to 0.56 and from 0.43 to 0.62, respectively (Table 4). Additionally, the concentrations of C_{21-22} steranes (i.e., pregnane and homopregnane) vary significantly compared to C_{27-29} steranes with C_{21-22}/(C_{21-22} + C_{27-29}) steranes ratios ranging from 0.03 to 0.39 (0.11 on average) (Table 4). The abundances of C_{27} diasteranes are also variable, with C_{27} diasteranes/(diasteranes + regular steranes) ratios ranging between 0.10 and 0.31 (avg. 0.19) (Table 4). Furthermore, detectable levels of C_{30} 4-methylsteranes are also observed (Figure 5e,f).

https://doi.org/10.1021/acsomega.4c08477
ACS Omega 2025, 10, 2735−2761

Table 2. Biomarker Parameters of Alkanes and β-Carotane of the Oil and EOM Samples from the Qigu Formation in the Yongjin Area of the Junggar Basin, China[a]

sample type	well	depth (m)	Pr/Ph	Pr/n-C_{17}	Ph/n-C_{18}	CPI	OEP	TAR	P_{aq}	β-carotane/n-C_{max}
Oil	Y 1	5873.40−5888.10	1.63	0.44	0.26	1.07	1.04	0.33	0.80	n.d.
	Y 1	5873.40−5888.10	1.84	0.46	0.25	1.05	1.01	0.31	0.79	n.d.
	Y 3	5609.60−5619.90	1.92	0.37	0.19	1.06	1.02	0.37	0.78	n.d.
	Y 301	5541.60−5552.00	1.50	0.36	0.20	1.03	1.04	0.11	0.93	0.01
	Y 301	5541.60−5552.00	1.76	0.30	0.18	1.04	1.05	0.04	0.94	0.00
	Y 302	5549.90−5655.80	0.98	0.37	0.23	1.04	1.04	0.17	0.93	0.01
	Y 302	5649.90−5666.30	1.46	0.27	0.21	1.03	1.06	0.04	0.94	0.00
	Y 3-x11	6021.00−6034.50	1.21	0.34	0.20	1.04	1.05	0.14	0.93	0.01
	Y 3-x11	6021.00−6034.50	1.70	0.29	0.18	1.03	1.05	0.04	0.94	0.00
	Y 3-x12	5784.20−5796.00	1.12	0.38	0.21	1.04	0.98	0.14	0.92	0.01
	Y 3-x12	5784.20−5796.00	1.63	0.29	0.19	1.02	1.05	0.04	0.93	0.00
	Y 3-cp1	5775.85−6110.80	1.76	0.30	0.19	1.05	1.06	0.04	0.94	0.00
EOM	Y 1−1	5814.43	n.d.	n.d.	n.d.	n.d.	n.d.	n.d.	n.d.	n.d.
	Y 1−1	5818.40	0.52	0.95	1.55	1.07	1.05	0.12	0.83	0.06
	Y 1−1	5822.57	n.d.	n.d.	n.d.	n.d.	n.d.	n.d.	n.d.	n.d.
	Y 1−1	5827.10	0.64	0.76	1.15	1.03	1.02	0.34	0.76	0.02
	Y 1−1	5839.10	0.37	0.35	1.24	1.07	1.03	0.08	0.76	0.27
	Y 1−1	5843.90	0.49	0.48	1.25	0.99	1.05	0.01	0.98	0.00
	YJ 1−3	5971.20	0.19	0.51	1.48	0.90	1.12	0.15	0.74	0.09
	YJ 1−3	5976.20	0.64	1.00	1.65	1.07	1.04	0.11	0.80	0.01
	YJ 1−3	5978.50	0.52	0.99	1.76	1.05	1.06	0.02	0.84	0.01
	YJ 1−3	5982.15	0.71	1.08	2.00	0.94	1.15	0.00	0.86	0.00
	YJ 1−3	5987.85	0.56	0.86	1.56	0.95	0.96	0.03	0.85	0.14
	YJ 1−3	5988.89	0.45	0.87	1.81	1.00	1.01	0.12	0.85	0.01
	YJ 1−3	5988.90	0.31	0.31	0.96	1.04	1.01	0.03	0.81	0.02
	YJ 1−3	5990.50	0.61	0.91	1.63	1.02	1.06	0.01	0.83	0.02
	YJ 1−3	5999.50	0.46	0.81	1.20	1.06	1.06	0.47	0.87	0.00
	Y 1	5874.50	1.51	0.44	0.24	1.06	1.04	0.48	0.79	n.d.
	Y 1	5878.10	1.71	0.44	0.24	1.07	1.04	0.45	0.77	n.d.
	Y 1	5880.00	1.57	0.47	0.27	1.05	1.03	0.41	0.79	n.d.
	Y 1	5886.50	1.47	0.44	0.26	1.10	1.05	0.61	0.70	n.d.
	Y 2	5998.00	1.54	0.49	0.29	1.05	1.03	0.45	0.74	n.d.
	Y 2	6000.60	0.94	0.24	0.21	1.08	1.07	0.52	0.79	0.02
	Y 2	6002.00	1.39	0.41	0.26	1.07	1.05	0.50	0.73	n.d.
	Y 2	6004.28	0.72	1.00	1.65	1.09	1.06	0.03	0.77	0.00
	Y 2	6004.45	0.89	0.32	0.27	0.95	0.99	0.06	0.91	0.01
	Y 2	6004.50	1.43	0.41	0.26	1.05	1.02	0.51	0.70	n.d.
	Y 3	5615.50	0.97	0.37	0.38	1.03	1.03	0.11	0.87	n.d.
	Y 3	5619.00	0.80	0.34	0.30	1.06	1.03	0.46	0.83	0.21
	Y 6	6027.40	0.68	0.53	0.95	1.09	1.05	2.77	0.75	0.19
	Y 6	6028.50	0.65	0.60	0.49	1.07	1.03	0.71	0.80	0.27
	Y 6	6033.20	1.02	0.84	1.18	1.13	1.07	0.35	0.72	0.16
	Y 6	6034.00	0.63	0.54	0.79	1.06	1.04	0.76	0.68	n.d.
	Y 6	6035.00	0.59	0.63	0.62	1.07	1.04	0.65	0.75	0.39
	Y 7	6099.80	1.04	1.02	1.51	1.03	1.05	0.01	0.80	0.00
	Y 8	6045.00	0.91	0.35	0.35	1.06	1.04	0.48	0.74	n.d.
	YJ 12	5767.90	0.37	0.30	0.88	1.08	1.05	0.32	0.81	0.13
	YJ 12	5772.95	0.47	0.70	1.45	0.98	1.02	0.02	0.98	0.00
	YJ 12	5774.37	0.35	0.29	1.10	1.08	1.05	0.04	0.78	0.00
	YJ 12	5783.30	0.69	0.76	0.79	1.08	1.04	0.64	0.85	0.00
	YJ 12	5785.40	0.47	0.28	0.49	1.09	1.05	0.80	0.75	0.05
	YJ 14	5486.00	0.49	0.44	0.99	1.08	1.04	0.23	0.74	0.42
	YJ 14	5517.50	0.26	0.45	1.27	1.02	1.02	0.03	0.87	0.01
	YJ 15	5780.00	0.32	0.39	1.19	1.08	1.05	0.24	0.83	0.17
	Y 301	5542.40	0.64	0.45	0.75	1.10	1.05	0.77	0.76	0.13
	Y 301	5543.60	0.68	0.70	0.58	1.08	1.06	0.84	0.86	0.00
	Y 301	5549.10	0.68	0.58	0.58	1.09	1.05	0.43	0.86	0.00
	YJ 302	5651.00	0.30	0.32	0.99	1.08	1.05	0.19	0.77	0.10
	YJ 303	5741.00	0.32	0.38	1.01	1.09	1.05	0.68	0.78	0.12
	YJ 303	5750.30	0.28	0.42	1.14	1.04	1.07	0.02	0.85	0.00

https://doi.org/10.1021/acsomega.4c08477
ACS Omega 2025, 10, 2735−2761

Table 2. continued

sample type	well	depth (m)	Pr/Ph	Pr/n-C_{17}	Ph/n-C_{18}	CPI	OEP	TAR	P_{aq}	β-carotane/n-C_{max}
	Y 3-x17	5722.50	0.38	0.31	0.85	1.07	1.05	0.29	0.76	0.08

[a]n.d., no detected; Pr, pristane; Ph, phytane; CPI = 2 × ∑odd n-C_{23-29}/(∑even n-C_{22-28} + ∑even n-C_{24-30}); OEP = (n-C_{21} + 6 × n-C_{23} + n-C_{25})/(4 × n-C_{22} + 4 × n-C_{24}); TAR = (n-C_{27} + n-C_{29} + n-C_{31})/(n-C_{15} + n-C_{17} + n-C_{19}); P_{aq} = (n-C_{23} + n-C_{25})/(n-C_{23} + n-C_{25} + n-C_{29} + n-C_{31}).

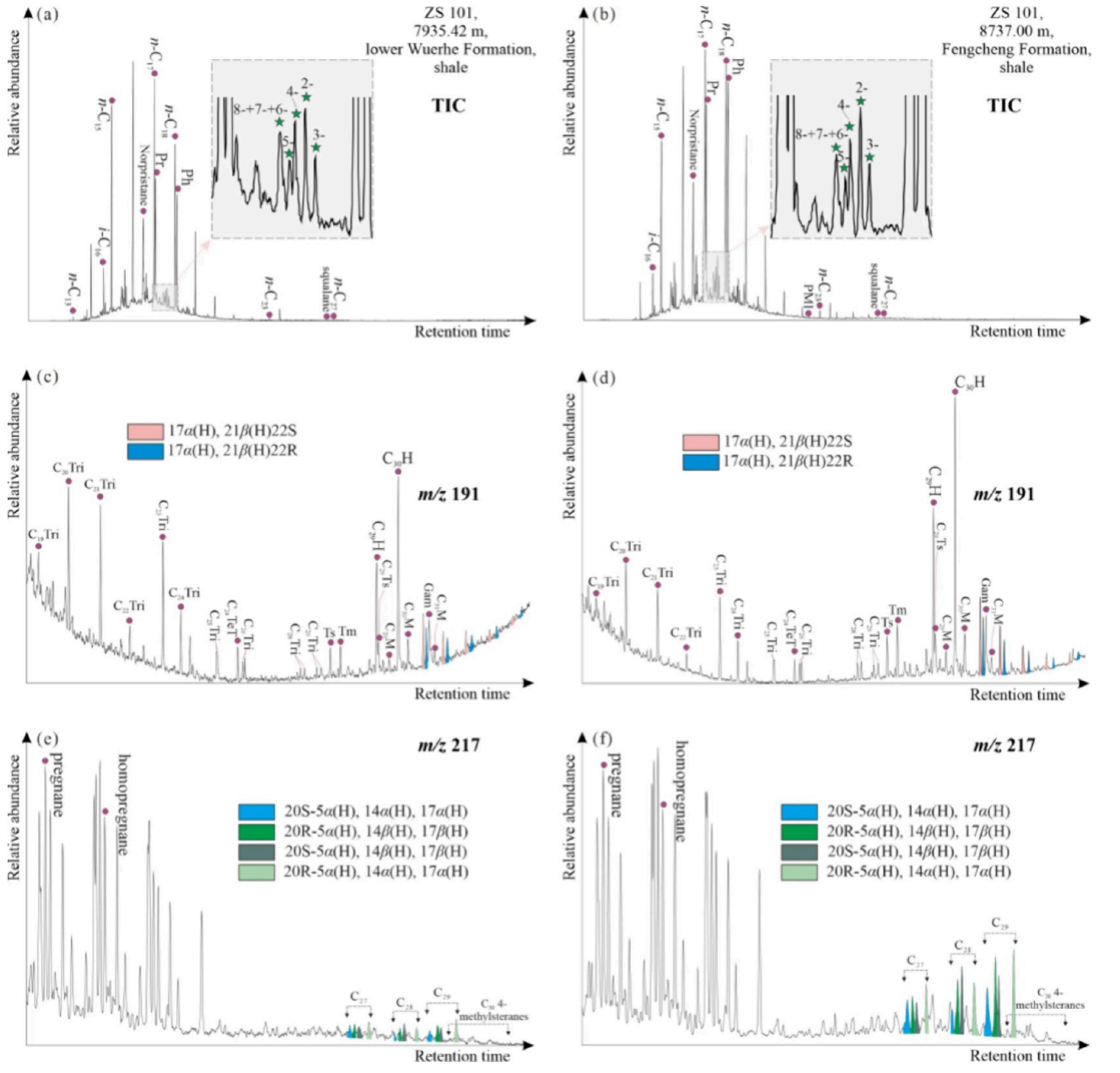

Figure 6. Distribution of partial mass chromatograms of the aliphatic fraction in representative samples (figures on the left represent source rocks from the Fengcheng Fm., and those on the right represent those from the lower Wuerhe Fm). (a, b) TIC, (c, d) mass chromatograms showing the distributions of hopanes (m/z 191) and (e, f) mass chromatograms showing the distributions of steranes (m/z 217).

The steranes are abundant in C_{21-22} steranes compared to C_{27-29} steranes in the source rocks (Figure 6e,f), and the parameters related to steranes are listed in Table 3.

4.2.4. Aromatic Hydrocarbons. The representative aromatic fraction for the Jurassic samples is depicted in Figure 7. The naphthalene (N; m/z 128) exhibits relatively low abundances (Figure 7). Among the homologues of trimethylnaphthalenes (TMNs; m/z 170), 1,3,6-TMN or 1,2,5-TMN is predominant in most samples with TNR-2 (calculated as (2,3,6- + 1,3,7-TMN)/(1,4,6- + 1,3,5- + 1,3,6-TMN))[26] ranging from 0.44 to 1.19 and log (1,2,5-TMN/1,3,6-TMN) from −0.46 to 0.60 (Table 5). The methyldibenzothiophenes (MDBTs; m/z 198) are predominantly comprised of 4-MDBT, with the MDR (4-MDBT/1-MDBT)[26] being between 1.32 and 7.53 (Table 5). Additionally, the distribution of tetramethylnaphthalenes (TeMNs; m/z 184) is characterized by the prevalence of 1,3,6,7-TeMN and 1,2,5,7- + 1,3,6,8-TeMN. The methylphenanthrenes (MPs; m/z 192) distributions are characterized by

https://doi.org/10.1021/acsomega.4c08477
ACS Omega 2025, 10, 2735−2761

Table 3. Biomarker Parameters of Aliphatic Fractions of the Source Rocks from the Fengcheng and Lower Wuerhe Samples from the ZS 101 Well in the Yongjin Area of the Junggar Basin, China[a]

formation	depth (m)	Pr/Ph	Pr/n-C_{17}	Ph/n-C_{18}	C_{20}/C_{23}Tri	Gamm/C_{30} Hop	C_{27}/C_{29} $\alpha\alpha\alpha$20R sterane	hopanoids/steranes
lower Wuerhe	7935.42	0.92	0.57	0.91	1.05	0.28	1.02	2.77
	7941.00	0.91	0.52	0.72	0.60	0.20	1.00	0.98
	7944.74	1.01	0.47	0.62	2.19	0.30	1.09	2.88
	7947.40	1.35	0.71	1.11	2.16	0.25	0.67	2.51
	7955.40	0.56	0.52	0.99	1.54	0.19	0.67	3.44
Fengcheng	8445.00	0.69	0.54	0.91	2.99	0.07	1.24	4.67
	8575.00	0.84	0.51	0.84	0.65	0.10	1.51	5.00
	8664.50	0.61	0.51	0.89	1.34	0.06	1.37	4.54
	8634.50	0.42	0.30	0.76	1.94	0.08	1.24	3.64
	8737.00	0.73	0.53	0.84	1.01	0.26	0.42	2.00
	8742.50	0.80	0.53	0.84	1.43	0.17	0.69	2.44
	8956.70	0.87	0.54	0.90	1.67	0.20	0.81	2.91
	8958.35	0.80	0.64	0.96	1.11	0.27	0.50	3.30

[a]Pr, pristane; Ph, phytane; Tri, tricyclic terpane; Hop, hopane; Gamm, Gammacerane.

MPI-1 (calculated as 1.5 × (3- + 2-MP)/(P + 9- + 1-MP);[27] MNR (2-MN/1-MN), F1 (calculated as (3- + 2-MP)/(2- + 3- + 1- + 9-MP)),[28] and F2 (calculated as (2-MP)/(2- + 3- + 1- + 9-MP))[28] are 0.27−1.17, 0.75−2.06, 0.33−0.56, and 0.19−0.32, respectively (Table 5). Furthermore, ethylphenanthrenes + dimethylphenanthrenes (EPs + DMPs; m/z 206), trimethylphenanthrenes (TMPs, m/z 220), retene (m/z 219), chrysene (m/z 228), fluoranthene and pyrene (m/z 202), as well as benzo[b]fluoranthene, benzo[a]pyrene, benzo[e]pyrene, and perylene (m/z 252) are observed (Figure 7).

The normalized distribution of dibenzothiophene (DBT; m/z 184), fluorene (Fl; m/z 166), and dibenzofurane (DBF; m/z 168) shows that DBT occurs in the highest relative concentration (18.07−92.95%) in comparison to DBF (1.54−63.73%) and FL (2.93−55.58%) (Table 5). In addition, DBT/PHE ratios range between 0.04 and 0.25 (Table 5).

Triaromatic steroids (TAS; m/z 231) as well as methyltriaromatic steroids and C_{29} 4α, 23,24-trimethyltriaromatic steroids (MeTAS and dino-TAS; m/z 245) are shown in Figure 8 with the C_{26}/C_{28} 20S TAS ratio, TAS cracking ratios (defined as (C_{20} + C_{21})/(C_{20} + C_{21} + C_{26} + C_{27} + C_{28}) TAS) and C_{20}/C_{20} + C_{28} (20R) TAS being 0.11−0.39, 0.07−0.43 and 0.19−0.66, respectively (Table 5).

4.3. Stable Organic Carbon Isotope Compositions. The $\delta^{13}C$ compositions of the oil and EOM samples ($\delta^{13}C_{oil/EOM}$) are ranging from −31.8 to −28.4‰ (Table 6). The $\delta^{13}C$ for aliphatic ($\delta^{13}C_{Sat}$) and aromatic ($\delta^{13}C_{Aro}$) hydrocarbons, NSO components ($\delta^{13}C_{NSO}$) and asphaltene ($\delta^{13}C_{Asp}$) vary from −32.2 to −29.7‰, −31.6 to −27.8‰, −30.2 to −27.6‰, and −31.0 to −28.1‰, respectively (Table 6).

5. DISCUSSION

The composition of crude oil is predominantly determined by factors including thermal maturity, depositional environment, origin of OM, and subsequent alteration process.[29]

5.1. Thermal Maturity. The assessment of oil thermal maturity involves the interpretation of molecular maturity indicators obtained from aliphatic and aromatic hydrocarbons. Specifically, the evaluation of the C_{31} and C_{32} homohopanes 22S/(22S + 22R) ratio suggests that the oils have reached the main oil window in terms of thermal maturity (Figure 9a).[27] Similarly, the C_{29} $\alpha\alpha\alpha$ 20S/(20S + 20R) to $\beta\beta$/($\beta\beta$ + $\alpha\alpha$) steranes ratios yield comparable indications regarding thermal maturity (Figure 9b).

The distributions of MPs are primarily affected by thermal maturity, and they are less affected by lithology and kerogen types.[28] Consequently, they are commonly utilized as thermal maturity parameters, such as MPI-1, MNR, F1, and F2, as well as their calculated VR_r. The MPI-1 and MNR values suggest that the thermal maturities of the oil and EOM samples are within the main oil window (Figure 10a). Similar conclusions can be drawn from the cross plot of F1 vs F2 and the calculated VR_r based on F2 (see Figure 10b). Other aromatic maturity-related parameters, including TNR-2[30] and MDR,[26] as well as their respective calculated VR_r (Table 4), also indicate the thermal maturity of the crude oil and EOM samples in the main stage of the oil window (Figure 11a).

The C_{26}/C_{28} 20S TAS ratio, TAS cracking ratios and C_{20}/C_{20} + C_{28} (20R) TAS are commonly used as thermal maturity indicators.[32,33] The distributions of TAS indicate the thermal maturity of the oil and EOM samples is in the early to middle oil window stage (Figure 11b).

5.2. Depositional Setting. The interpretation of depositional settings of the related source rocks of the oils can be facilitated by analyzing various molecular parameters. The source rocks deposited under lacustrine settings can be inferred from higher abundances of C_{30} Hop relative to C_{29} Hop, as well as low C_{22}/C_{21} and high C_{24}/C_{23} Tri ratios (Figure 12a).[34] It should be noted that the C_{29}/C_{30} Hop ratio is greater than 0.8 in some samples, which actually indicates that the shale, composed of carbonate and marlstone matrix, deposited under lacustrine conditions with high salinity (see below).[35,36] Additionally, nonfresh water in lacustrine settings can be deduced from the cross plot of C_{26}/C_{25} Tri vs C_{31} 22R/C_{30} Hop ratios (Figure 12b).[27] The identification of clay-bearing source rocks can be achieved by analyzing the cross plot of $C_{21-22}/(C_{21-22} + C_{27-29})$ steranes vs C_{27} diasteranes/(diasteranes + regular steranes) (Figure 13a).[37,38] Furthermore, the deposition of the source rocks in clastic facies can be discerned by the gradual decrease from C_{31} to C_{35} Hop (Figure 4c,d).[37] The ratio of Ts/(Ts + Tm) vs C_{27} diasteranes/(diasteranes + regular steranes) (Figure 13b) may be affected by the thermal maturity of OM and lithology.[27,39−41] Notably, the low values of both Ts/(Ts + Tm) and C_{27} diasteranes/(diasteranes + regular steranes) compared to those in the Triassic Yanchang Fm. source rocks (see ref 37 for details) indicate that the related source rocks of the oils developed fewer clay minerals. Additionally, the occurrence of detectable 4-methylsteranes further supports the

https://doi.org/10.1021/acsomega.4c08477
ACS Omega 2025, 10, 2735−2761

Table 4. Biomarker Parameters of Tricyclic and Tetracyclic Terpanes, Hopanes, and Steranes of the Oil and EOM Samples from the Qigu Formation in the Yongjin Area of the Junggar Basin, China[a]

			Tris and Tet						hop						
sample type	well	depth (m)	C_{22}/C_{21} Tri	C_{24}/C_{23}Tri	C_{26}/C_{25}Tri	C_{24} Tet/C_{23} Tri	$C_{19}/(C_{19}+C_{23})$ Tri	ETR	Ts/(Ts + Tm)	C_{29}/C_{30} hop	Gamm/C_{30} hop	C_{31} 22R/C_{30} hop	C_{31} hop S/(S + R)	C_{32} hop S/(S + R)	C_{29} NH/C_{30} hop
Oil	Y 1	5873.40−5888.10	0.23	0.50	1.17	0.31	0.15	2.00	0.43	0.62	0.48	0.27	0.50	0.55	n.d.
	Y 1	5873.40−5888.10	0.23	0.52	1.27	0.33	0.17	2.48	0.43	0.64	0.48	0.27	0.50	0.55	n.d.
	Y 3	5609.60−5619.90	0.23	0.52	1.28	0.36	0.19	2.00	0.44	0.63	0.46	0.27	0.51	0.55	n.d.
	Y 301	5541.60−5552.00	0.22	0.52	1.19	0.18	0.22	2.52	0.42	0.70	0.35	0.23	0.52	0.56	0.39
	Y 301	5541.60−5552.00	0.18	0.45	0.90	0.19	0.28	2.62	0.41	0.84	0.29	0.18	0.57	0.56	0.39
	Y 302	5549.90−5655.80	0.24	0.51	1.19	0.17	0.16	2.74	0.46	0.73	0.42	0.25	0.49	0.55	0.53
	Y 302	5649.90−5666.30	0.18	0.50	1.08	0.17	0.25	2.92	0.46	0.80	0.34	0.22	0.54	0.65	0.45
	Y 3-x11	6021.00−6034.50	0.23	0.52	1.34	0.18	0.20	2.35	0.41	0.70	0.33	0.22	0.51	0.54	0.40
	Y 3-x11	6021.00−6034.50	0.17	0.46	1.73	0.19	0.29	2.25	0.45	0.84	0.27	0.19	0.55	0.58	0.36
	Y 3-x12	5784.20−5796.00	0.23	0.49	1.52	0.19	0.22	2.24	0.42	0.70	0.33	0.23	0.51	0.55	0.39
	Y 3-x12	5784.20−5796.00	0.17	0.47	0.96	0.19	0.29	2.51	0.41	0.78	0.28	0.17	0.59	0.63	0.36
	Y 3-cp1	5775.85−6110.80	0.18	0.48	1.18	0.19	0.30	2.33	0.45	0.79	0.27	0.18	0.59	0.62	0.36
EOM	Y 1−1	5814.43	0.23	0.53	1.57	0.34	0.13	2.38	0.34	0.86	0.44	0.22	0.54	0.61	n.d.
	Y 1−1	5818.40	0.24	0.53	1.47	0.29	0.13	1.86	0.38	0.62	0.47	0.24	0.52	0.55	0.45
	Y 1−1	5822.57	0.23	0.54	1.25	0.34	0.14	2.04	0.38	0.80	0.48	0.29	0.54	0.58	n.d.
	Y 1−1	5827.10	0.21	0.51	1.28	0.29	0.14	1.72	0.40	0.75	0.23	0.14	0.58	0.61	0.12
	Y 1−1	5839.10	0.22	0.54	1.40	0.41	0.15	1.40	0.35	0.60	0.32	0.20	0.56	0.57	0.03
	Y 1−1	5843.90	0.18	0.43	1.15	0.19	0.29	1.53	0.42	0.84	0.14	0.17	0.56	0.59	0.18
	YJ 1−3	5971.20	0.26	0.55	1.40	0.40	0.12	1.53	0.44	0.83	0.57	0.26	0.54	0.59	0.27
	YJ 1−3	5976.20	0.22	0.54	1.42	0.40	0.31	1.49	0.36	0.67	0.40	0.28	0.53	0.57	0.20
	YJ 1−3	5978.50	0.23	0.53	1.38	0.32	0.22	1.74	0.35	0.75	0.50	0.29	0.50	0.56	0.38
	YJ 1−3	5982.15	0.15	0.43	1.27	0.32	0.64	1.60	0.23	1.15	0.33	0.36	0.55	0.55	0.06
	YJ 1−3	5987.85	0.23	0.54	1.39	0.30	0.11	1.95	0.39	0.62	0.58	0.22	0.52	0.58	0.34
	YJ 1−3	5988.89	0.22	0.51	1.34	0.28	0.12	2.12	0.41	0.84	0.34	0.16	0.57	0.60	0.37
	YJ 1−3	5988.90	0.22	0.51	1.32	0.38	0.21	1.61	0.42	0.77	0.49	0.27	0.53	0.58	0.23
	YJ 1−3	5990.50	0.21	0.53	1.16	0.34	0.16	1.16	0.60	0.85	1.04	0.23	0.54	0.56	0.31
	YJ 1−3	5999.50	0.23	0.50	1.36	0.29	0.13	2.28	0.37	0.83	0.26	0.17	0.56	0.64	0.44
	Y 1	5874.50	0.24	0.50	1.26	0.31	0.14	2.84	0.41	0.60	0.45	0.26	0.50	0.55	n.d.
	Y 1	5878.10	0.23	0.52	1.19	0.35	0.16	2.54	0.41	0.57	0.44	0.27	0.50	0.58	n.d.
	Y 1	5880.00	0.23	0.53	1.35	0.34	0.16	2.32	0.42	0.62	0.37	0.26	0.51	0.57	n.d.
	Y 1	5886.50	0.22	0.48	1.35	0.33	0.16	2.48	0.43	0.60	0.44	0.26	0.51	0.57	n.d.

https://doi.org/10.1021/acsomega.4c08477
ACS Omega 2025, 10, 2735−2761

Table 4. continued

sample type	well	depth (m)	Tris and Tet						hop						
			C_{22}/C_{21} Tri	C_{24}/C_{23}Tri	C_{26}/C_{25}Tri	C_{24} Tet/C_{23} Tri	$C_{19}/(C_{19}+C_{23})$ Tri	ETR	Ts/(Ts + Tm)	C_{29}/C_{30} hop	Gamm/C_{30} hop	C_{31} 22R/C_{30} hop	C_{31} hop S/(S + R)	C_{32} hop S/(S + R)	C_{29} NH/C_{30} hop
	Y 2	5998.00	0.23	0.52	1.39	0.32	0.19	1.72	0.35	0.61	0.29	0.29	0.55	0.57	n.d.
	Y 2	6000.60	0.22	0.51	1.20	0.47	0.28	1.00	0.38	0.64	0.24	0.27	0.54	0.58	0.13
	Y 2	6002.00	0.24	0.55	1.29	0.32	0.21	1.86	0.47	0.55	0.41	0.23	0.53	0.55	n.d.
	Y 2	6004.28	0.20	0.45	1.09	0.13	0.31	1.60	0.43	0.65	0.33	0.21	0.57	0.57	0.13
	Y 2	6004.45	0.17	0.36	1.32	0.18	0.48	0.80	0.41	0.62	0.31	0.30	0.56	0.57	0.09
	Y 2	6004.50	0.23	0.52	1.33	0.31	0.21	1.87	0.48	0.53	0.43	0.24	0.53	0.55	n.d.
	Y 3	5615.50	0.20	0.48	1.15	0.24	0.29	1.86	0.51	0.59	0.44	0.25	0.52	0.59	n.d.
	Y 3	5619.00	0.22	0.51	1.33	0.36	0.14	1.65	0.38	0.76	0.43	0.24	0.52	0.59	0.35
	Y 6	6027.40	0.24	0.57	1.34	0.39	0.10	1.73	0.39	0.51	0.66	0.25	0.53	0.56	0.34
	Y 6	6028.50	0.22	0.49	1.33	0.33	0.12	2.37	0.35	0.75	0.55	0.23	0.51	0.58	1.07
	Y 6	6033.20	0.22	0.50	1.44	0.25	0.15	1.66	0.36	0.64	0.62	0.23	0.50	0.55	0.70
	Y 6	6034.00	0.24	0.58	1.16	0.37	0.14	2.24	0.48	0.40	0.72	0.25	0.53	0.56	n.d.
	Y 6	6035.00	0.23	0.51	1.27	0.32	0.11	2.38	0.34	0.83	0.56	0.27	0.48	0.58	0.96
	Y 7	6099.80	0.19	0.40	0.98	0.12	0.34	1.54	0.41	0.63	0.27	0.22	0.57	0.55	0.10
	Y 8	6045.00	0.27	0.58	1.42	0.35	0.17	2.56	0.55	0.55	0.61	0.24	0.50	0.59	n.d.
	YJ 12	5767.90	0.21	0.53	1.30	0.39	0.19	1.49	0.36	0.63	0.36	0.19	0.56	0.57	0.26
	YJ 12	5772.95	0.16	0.50	1.15	0.26	0.35	1.81	0.36	0.89	0.18	0.20	0.59	0.59	0.26
	YJ 12	5774.37	0.15	0.40	1.16	0.34	0.67	1.35	0.29	0.68	0.24	0.29	0.54	0.59	0.08
	YJ 12	5783.30	0.20	0.51	1.18	0.42	0.26	1.10	0.46	0.86	0.15	0.19	0.62	0.61	0.07
	YJ 12	5,785.40	0.22	0.55	1.36	0.49	0.21	0.97	0.41	0.66	0.20	0.25	0.57	0.58	0.02
	YJ 14	5486.00	0.22	0.53	1.31	0.32	0.13	2.21	0.34	0.75	0.51	0.21	0.54	0.57	0.68
	YJ 14	5517.50	0.18	0.39	1.12	0.26	0.44	1.33	0.32	0.67	0.29	0.26	0.55	0.58	0.11
	YJ 15	5780.00	0.23	0.53	1.34	0.33	0.12	1.84	0.41	0.72	0.48	0.24	0.52	0.61	0.37
	Y 301	5542.40	0.25	0.52	1.37	0.39	0.13	1.69	0.34	0.71	0.34	0.23	0.54	0.57	0.27
	Y 301	5543.60	0.23	0.51	1.27	0.32	0.13	1.87	0.39	0.82	0.24	0.14	0.61	0.60	0.37
	Y 301	5549.10	0.22	0.48	1.23	0.29	0.17	1.81	0.38	0.76	0.30	0.17	0.59	0.59	0.32
	YJ 302	5651.00	0.23	0.55	1.39	0.30	0.12	2.37	0.42	0.80	0.58	0.19	0.60	0.58	0.58
	YJ 303	5741.00	0.24	0.54	1.37	0.41	0.15	1.58	0.35	0.61	0.34	0.23	0.55	0.58	0.17
	YJ 303	5750.30	0.19	0.49	1.21	0.37	0.37	1.61	0.30	0.66	0.28	0.24	0.55	0.58	0.14
	Y 3-x17	5722.50	0.22	0.51	1.32	0.38	0.17	1.45	0.35	0.68	0.35	0.21	0.55	0.58	0.30

sample type	well	depth (m)	steranes						hopanoids/steranes
			C_{27}[b]	C_{28}[b]	C_{29}[b]	C_{29} $\alpha\alpha$ S/(S + R)	C_{29} $\beta\beta/(\beta\beta+\alpha\alpha)$	$C_{21-22}/(C_{21-22}+C_{27-29})$	C_{27} d/(d+r)[c]	
Oil	Y 1	5873.40−5888.10	11.18	42.98	45.84	0.55	0.56	0.04	0.20	1.47
	Y 1	5873.40−5888.10	13.48	41.12	45.39	0.55	0.56	0.05	0.17	1.49
	Y 3	5609.60−5619.90	14.11	39.63	46.26	0.53	0.54	0.06	0.18	2.05
	Y 301	5541.60−5552.00	23.62	37.90	38.47	0.48	0.52	0.16	0.17	1.16
	Y 301	5541.60−5552.00	18.93	41.63	39.44	0.52	0.62	0.24	0.29	1.22
	Y 302	5549.90−5655.80	22.81	37.27	39.93	0.47	0.53	0.17	0.21	1.25
	Y 302	5649.90−5666.30	19.57	43.01	37.42	0.51	0.60	0.25	0.31	1.28
	Y 3-x11	6021.00−6034.50	23.01	37.67	39.32	0.49	0.53	0.15	0.18	1.32

https://doi.org/10.1021/acsomega.4c08477
ACS Omega 2025, 10, 2735−2761

Table 4. continued

			steranes							
sample type	well	depth (m)	C_{27}[b]	C_{28}[b]	C_{29}[b]	C_{29} $\alpha\alpha$ S/(S + R)	C_{29} $\beta\beta/(\beta\beta + \alpha\alpha)$	$C_{21-22}/(C_{21-22} + C_{27-29})$	C_{27} d/(d+r)[c]	hopanoids/steranes
	Y 3-x11	6021.00−6034.50	21.41	39.29	39.31	0.55	0.60	0.23	0.30	1.32
	Y 3-x12	5784.20−5796.00	23.69	36.15	40.16	0.49	0.53	0.16	0.17	1.38
	Y 3-x12	5784.20−5796.00	19.89	40.09	40.02	0.50	0.60	0.24	0.27	1.39
	Y 3-cp1	5775.85−6110.80	20.14	39.55	40.31	0.55	0.58	0.24	0.31	1.28
EOM	Y 1−1	5814.43	17.95	42.62	39.42	0.50	0.57	0.06	0.12	1.26
	Y 1−1	5818.40	19.66	36.35	43.99	0.56	0.48	0.05	0.10	1.17
	Y 1−1	5822.57	16.82	42.34	40.85	0.50	0.57	0.06	0.16	1.55
	Y 1−1	5827.10	15.92	43.00	41.07	0.51	0.59	0.12	0.20	2.57
	Y 1−1	5839.10	14.45	39.94	45.61	0.48	0.55	0.05	0.11	3.97
	Y 1−1	5843.90	27.29	38.27	34.44	0.50	0.55	0.32	0.29	0.17
	YJ 1−3	5971.20	18.44	38.40	43.16	0.49	0.60	0.06	0.16	4.11
	YJ 1−3	5976.20	19.54	33.66	46.80	0.52	0.51	0.05	0.12	1.81
	YJ 1−3	5978.50	20.48	36.34	43.18	0.50	0.51	0.06	0.10	1.50
	YJ 1−3	5982.15	27.11	30.61	42.28	0.47	0.45	0.18	0.18	5.63
	YJ 1−3	5987.85	18.39	36.97	44.64	0.54	0.47	0.05	0.17	5.11
	YJ 1−3	5988.89	15.36	43.60	41.04	0.50	0.58	0.10	0.18	1.46
	YJ 1−3	5988.90	20.81	36.54	42.66	0.46	0.57	0.08	0.15	4.08
	YJ 1−3	5990.50	20.32	40.18	39.50	0.53	0.50	0.11	0.21	3.39
	YJ 1−3	5999.50	14.70	43.92	41.38	0.52	0.61	0.09	0.17	1.19
	Y 1	5874.50	14.21	40.35	45.45	0.54	0.56	0.05	0.31	1.56
	Y 1	5878.10	13.78	39.76	46.46	0.53	0.55	0.06	0.16	1.62
	Y 1	5880.00	14.70	39.32	45.98	0.54	0.56	0.06	0.19	1.66
	Y 1	5886.50	12.80	41.01	46.19	0.54	0.56	0.06	0.21	1.66
	Y 2	5998.00	15.39	36.77	47.83	0.51	0.51	0.06	0.21	2.63
	Y 2	6000.60	19.70	30.20	50.10	0.46	0.58	0.08	0.20	3.40
	Y 2	6002.00	16.05	37.87	46.08	0.54	0.55	0.07	0.22	2.06
	Y 2	6004.28	24.18	31.19	44.63	0.49	0.43	0.29	0.25	1.78
	Y 2	6004.45	19.33	25.71	54.95	0.42	0.57	0.19	0.22	5.62
	Y 2	6004.50	16.97	37.72	45.31	0.54	0.55	0.07	0.21	1.98
	Y 3	5615.50	17.36	36.90	45.74	0.53	0.54	0.12	0.23	1.87
	Y 3	5619.00	15.53	38.43	46.03	0.48	0.56	0.06	0.15	2.51
	Y 6	6027.40	22.75	31.79	45.46	0.47	0.50	0.03	0.14	1.70
	Y 6	6028.50	16.51	35.95	47.53	0.49	0.59	0.07	0.16	1.78
	Y 6	6033.20	17.15	39.69	43.16	0.51	0.51	0.06	0.17	0.94
	Y 6	6034.00	19.16	33.09	47.75	0.51	0.48	0.04	0.19	1.46
	Y 6	6035.00	16.25	35.68	48.07	0.48	0.58	0.06	0.15	1.50
	Y 7	6099.80	24.82	31.51	43.67	0.49	0.43	0.39	0.24	1.73
	Y 8	6045.00	22.83	35.05	42.12	0.56	0.52	0.04	0.20	1.20
	YJ 12	5767.90	15.63	39.28	45.09	0.48	0.56	0.05	0.12	2.54
	YJ 12	5772.95	22.75	41.15	36.09	0.46	0.58	0.16	0.19	1.76
	YJ 12	5774.37	28.17	29.21	42.62	0.45	0.50	0.14	0.17	4.69
	YJ 12	5783.30	20.72	36.26	43.02	0.49	0.60	0.11	0.22	3.17

https://doi.org/10.1021/acsomega.4c08477
ACS Omega 2025, 10, 2735−2761

Table 4. continued

sample type	well	depth (m)	steranes							hopanoids/steranes
			C_{27}[b]	C_{28}[b]	C_{29}[b]	C_{29} $\alpha\alpha$ S/(S + R)	C_{29} $\beta\beta$/($\beta\beta$ + $\alpha\alpha$)	C_{21-22}/(C_{21-22} + C_{27-29})	C_{27} d/(d+r)[c]	
	YJ 12	5,785.40	20.77	34.29	44.95	0.46	0.57	0.06	0.14	4.41
	YJ 14	5486.00	14.68	42.33	42.98	0.49	0.52	0.06	0.12	1.49
	YJ 14	5517.50	28.21	30.75	41.04	0.42	0.48	0.11	0.19	4.18
	YJ 15	5780.00	16.72	41.00	42.27	0.49	0.59	0.07	0.16	2.86
	Y 301	5542.40	16.87	39.26	43.86	0.47	0.57	0.05	0.14	2.36
	Y 301	5543.60	15.77	42.92	41.30	0.52	0.59	0.09	0.21	1.59
	Y 301	5549.10	16.20	41.54	42.25	0.50	0.59	0.10	0.20	1.76
	YJ 302	5651.00	16.32	41.40	42.27	0.51	0.53	0.06	0.14	2.11
	YJ 303	5741.00	17.15	38.12	44.73	0.49	0.57	0.05	0.13	2.52
	YJ 303	5750.30	21.75	35.92	42.33	0.46	0.55	0.07	0.17	2.94
	Y 3-x17	5722.50	16.31	39.88	43.81	0.47	0.55	0.06	0.15	2.34

[a]Tri, tricyclic terpane; Tet, tetracyclic terpane; Hop, hopane; C_{29}NH, C_{29} 25-norhopane; Gamm, Gammacerane; Hop S/(S + R) = hopane 22S/(22S + 22R); C_{27} (%) = 100 × [C_{27}/(C_{27} + C_{28} + C_{29}) regular steranes] (C_{28} and C_{29} in regular steranes obtained via similar calculation); C_{29} $\alpha\alpha\alpha$ S/(S + R) = C_{29} $\alpha\alpha\alpha$ 20S/(20S + 20R) regular sterane. [b]Normalized concentrations of C_{27}, C_{28}, and C_{29} steranes (%). [c]Diasteranes/(diasteranes + regular steranes).

inference of the lacustrine setting.[42] It should be noted that there is no clear distinction between oil and EOM samples, indicating that both were formed under a lacustrine setting.

The paleoredox state of the benthic water column can be inferred from various geochemical proxies such as the Pr/Ph ratio (e.g., refs 36,43−47). A Pr/Ph ratio >3 implies oxic environments with significant contributions from higher plants, while a ratio <0.8 suggests anoxic conditions with increasing input of algae, particularly in high salinity or carbonate sedimentary settings.[43] The analyzed samples display varying Pr/Ph ratios indicative of a distinct contrast in their related source rock properties with oils originating from suboxic to reducing environments, while EOM samples were formed under anoxic conditions. This difference is further illustrated by the Pr/n-C_{17} vs Ph/n-C_{18} diagram (Figure 14a). An increased salinity generally has an adverse effect on biodiversity and is beneficial to the preservation of OM postsedimentation in water columns.[48] The Gamm/C_{30} $\alpha\beta$ Hop ratio suggests that the related source rocks were deposited in saline to hypersaline environments with large variations in salinity (Figure 14b). This inference is supported by the substantial variations in the abundances of β-carotane which are regarded as an indicator of high salinity conditions (e.g., refs 27,49).

FLs, DBFs, and DBTs can be produced through the reactions of biphenyl or methyl-substituted biphenyls with surface-active methylene, oxygen, and sulfur species on carbon surfaces.[50] Furthermore, DBT is enriched in saline water conditions, while DBF is comparatively more abundant in freshwater environments.[51,52] The relative contributions of Fl, DBF, and DBT in the investigated samples serve as evidence that the related source rocks were deposited under high salinity conditions (Figure 15a). A similar result is further supported by the cross plot of DBT/PHE vs Pr/Ph (Figure 15b).

Furthermore, a high ETR value is a signature of high salinity situations and/or reducing conditions in the water column, signifying an OM contribution from algae.[53−55] For the investigated samples, the high values of ETR might stem from a comprehensive result influenced by high salinity and reducing conditions in the water column as well as algal input, as evidenced by the absence of a linear correlation between the ETR and Gamm/C_{30} $\alpha\beta$ Hop (Figure 16).

5.3. Origin of Organic Matter. Various types of hydrocarbon compounds can serve as reliable indicators of the biological origins of OM (e.g., refs 21,25,38,45,56,57).

The distributions of saturated hydrocarbons are important in identifying their biological sources. Short-chain n-alkanes (i.e., n-C_{12}−C_{18}) are primarily derived from algae and phytoplankton, especially with relatively high n-C_{17} or n-C_{18} concentrations indicating marine algae and cyanobacteria.[42,58−60] Intermediate-chain n-alkanes (n-C_{21-25}) are generally inductive of aquatic higher plants,[61] particularly pecking at n-C_{23} and n-C_{25} alkanes, which are associated with aquatic pollen taxa, Nymphaea, Sphagnum moss species, and fresh-water algae (e.g., refs 42,62−64). Additionally, long-chain n-alkanes with a clear odd−even carbon predominance generally suggest higher plant input,[65] and high concentrations of C_{27}, C_{29}, and C_{31} n-alkanes are indicative of land plant epicuticular waxes.[58] In contrast, long-chain n-alkanes without a clear odd−even carbon predominance indicate saltwater algae input.[36,37]

The P_{aq} values indicate that submerged/floating vegetation is the primary biological source of the OM.[61] Considering the thermal maturity of the oil and EOM samples, both the CPI and OEP values have lost their effectiveness in indicating the source

https://doi.org/10.1021/acsomega.4c08477
ACS Omega 2025, 10, 2735−2761

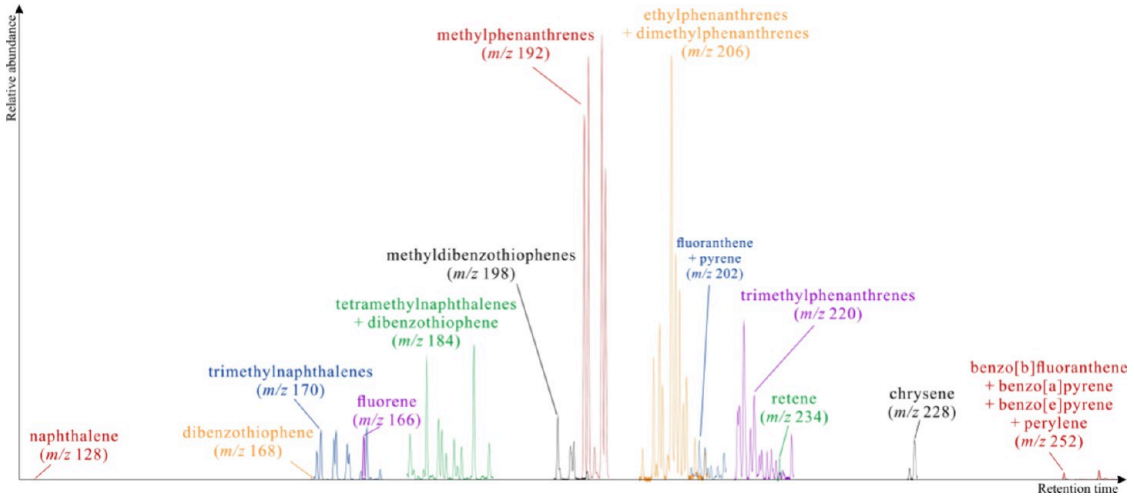

Figure 7. Partial mass chromatograms for the aromatic fraction of the oil sample from the Y 301 well.

of OM.[67] The low TAR, although it is affected by the thermal maturity of the OM, implies that aquatic organisms are a more significant biological source. Furthermore, the presence of branched alkanes, such as *i*-C_{15}, *i*-C_{16}, and *i*-C_{17}, indicates the biological contribution of bacteria.[68,69] Additionally, some species of algae and bacteria can be identified by some specific compounds in most samples, e.g., PMI, 3-MeHs, and squalene being inductive of methanogens, both the short-chain MMAs and 2-MeHs indicating the occurrence of cyanobacteria and C_{30} 4-methylsteranes being closely associated with dinoflagellates.[70−74] This finding can also be supported by the higher abundances of MeTAS and dino-TAS, as they are indicative of modern marine dinoflagellates (Figure 6).[27] The lower contributions of terrestrial higher plants to OM, compared to aquatic higher plants, are also supported by the low ratios of C_{24} Tet/C_{23} Tri and C_{19}/(C_{19} + C_{23}) Tri ratios (Table 3).[27,53,75−78]

In general, C_{27} and C_{28} steranes are signatures of zooplankton and phytoplankton, respectively.[66] In contrast, the origins of C_{29} steranes are more intricate, such as terrestrial plants input in freshwater conditions[66] as well as some aquatic plants and microalgae in high saline situations.[19,53,66,79,80] The ternary diagram illustrating the relative concentrations of C_{27}, C_{28}, and C_{29} steranes (Figure 17)[66] implies that the OM origins are sourced mainly from bacteria and algae deposited in bay/estuary environments. Considering the paleosalinity conditions, the high concentrations of C_{29} steranes are an indicator of inputs of aquatic plants and microalgae.

The relative contribution of prokaryotes compared to eukaryotes (such as higher plants and algae) can be estimated using the hopanoids/steranes ratio because hopanoids are derived from microbial cell membranes.[27,77,81] The hopanoids/steranes ratios ranging from 0.20 to 6.24 (avg. 2.34; Table 3) for the oil and EOM samples are higher than those in organic-rich sedimentary rocks and oils in the Phanerozoic marine,[27,37,82] indicating high levels of bacterial versus eukaryotic contribution.

Some certain compounds of TMNs are signatures of terrestrial higher plants, such as 1,2,5-TMN and 1,2,7-TMN.[83−86] The low concentrations of TMNs indicate a minimal OM contribution from terrestrial higher plants (Figure 7). 1-MP and 9-MP are connected to type III kerogen and type II−I kerogens, respectively.[87] Furthermore, retene and 1,7-DMP are linked to conifers.[88,89] The cross plots of log (1-MP/9-MP) vs log (1,2,5-TMN/1,3,6-TMN) (Figure 18a) and log (retene/9-MP) vs log [1,7-DMP/(1,3- + 3,9- + 2,10- + 3,10-DMP)] (Figure 18b) suggest a limited contribution of terrestrial OM, as most samples are distributed in the lower left quadrants. This result is further supported by the limited presence of typical signatures of terrestrial higher plants, including naphthalene, TMPs, chrysene, perylene, fluoranthene, pyrene, benzo[a]-pyrene, benzo[e]pyrene, benzo[b]fluoranthene, etc.[90−95]

The $\delta^{13}C_{Sat}$ and $\delta^{13}C_{Aro}$ values of the studied samples suggest that they are primarily nonmarine (waxy) oils (Figure 19a).[96] To distinguish OM derived from marine and terrestrial settings, the Canonical Variable (CV = $-2.53 \times \delta^{13}C_{Sat} + 2.22 \times \delta^{13}C_{Aro} - 11.65$)[96] was calculated, using a threshold value of <0.47 and >0.47 for discrimination. The CV values for the studied samples indicate that the OM is predominantly derived from terrestrial settings, with samples below the threshold potentially influenced by thermal maturity[97] and higher salinity. Furthermore, the CV values provide insights into water column stratifications.[97] Additionally, the Jurassic source rocks exhibit a heavier $\delta^{13}C$ composition with $\delta^{13}C$ values > −28‰ in contrast to the Permian source rocks with $\delta^{13}C$ values < −29‰, as the Permian source rocks have a larger contribution of sapropelic OM, but humic OM makes an important contribution to the Jurassic source rocks.[17,18,20,98] The $\delta^{13}C$ composition of the oil and EOM samples also indicates the sapropelic OM from the Permian source rocks is the major biological origins (Figure 19b).

5.4. Biodegradation Assessment. Generally, the presence of the unresolved complex mixture (UCM) in the TIC (Figure 5a,b) readily indicates that biodegradation occurred in the oil and EOM samples.[27,99] Microbial activity primarily targets normal and branched alkanes, as well as alkylated benzenes, resulting in their preferential consumption.[27] During the initial biodegradation stage, *n*-C_{8-12} compounds are significantly depleted.[27] The complete absence of *n*-$C_{<16}$ is characteristic of heavy to severe biodegradation (rank 3−4) in OM.[27] Sparse concentrations of *n*-$C_{<16}$ in the studied oil and EOM samples indicate moderate (rank 2) to heavy levels (rank 3) of biodegradation. Furthermore, high concentrations of isoprenoids (e.g., *i*-C_{16}, nor-pristine, Pr, and Ph) indicate their resistance to biodegradation, suggesting a biodegradation scale below rank 4, as complete consumption of isoprenoids occurs only in severe cases (rank > 4). However, the $C_{29}NH/C_{30}$ Hop ratios of most studied samples are above 0.1, and the presence of

https://doi.org/10.1021/acsomega.4c08477
ACS Omega 2025, 10, 2735−2761

Table 5. Parameters of Aromatic Fractions of the Oil and EOM Samples from the Qigu Formation in the Yongjin Area of the Junggar Basin, China[a]

sample type	well	depth (m)	TNR-2	MDR	MPI-1	MNR	F1	F2	VR_{MPI-1}	VR_{TNR-2}	VR_{MDR}
Oil	Y 1	5873.00−5881.00	0.86	4.62	0.80	1.39	0.47	0.26	0.92	0.91	0.85
	Y 1	5873.40−5888.10	0.95	5.66	0.79	1.59	0.48	0.26	0.92	0.97	0.92
	Y 1	5873.40−5888.10	1.19	5.82	0.83	1.55	0.49	0.27	0.95	1.11	0.94
	Y 3	5609.60−5619.90	0.68	6.81	0.91	1.28	0.51	0.27	1.00	0.81	1.01
	Y 301	5541.60−5552.00	0.85	6.80	0.90	1.54	0.50	0.27	0.99	0.91	1.01
	YJ 302	5549.90−5655.80	0.94	4.94	0.96	1.80	0.45	0.25	1.00	0.96	0.87
	Y 3-x11	6021.00−6034.50	0.93	6.01	0.97	2.06	0.50	0.27	1.03	0.96	0.95
	Y 3-x12	5784.20−5796.00	0.87	7.53	0.91	1.63	0.51	0.27	1.00	0.92	1.06
EOM	Y 1−1	5814.43	0.71	5.33	0.61	1.28	0.40	0.21	0.80	0.83	0.90
	Y 1−1	5818.40	0.64	3.96	0.70	1.28	0.45	0.26	0.86	0.78	0.80
	Y 1−1	5822.57	0.71	3.34	0.66	1.26	0.40	0.20	0.83	0.82	0.75
	Y 1−1	5839.10	0.62	3.13	0.48	1.77	0.36	0.23	0.71	0.77	0.74
	YJ 1−3	5971.20	0.89	2.84	0.73	1.83	0.45	0.26	0.88	0.94	0.72
	YJ 1−3	5976.20	0.79	5.40	0.86	1.38	0.50	0.28	0.97	0.87	0.90
	YJ 1−3	5978.50	0.70	3.86	0.83	1.43	0.49	0.27	0.94	0.82	0.79
	YJ 1−3	5982.15	0.76	5.21	0.42	1.11	0.45	0.27	0.69	0.86	0.89
	YJ 1−3	5987.85	0.44	2.22	0.50	1.15	0.35	0.24	0.72	0.66	0.67
	YJ 1−3	5988.90	0.90	3.55	0.80	1.84	0.47	0.27	0.92	0.94	0.77
	YJ 1−3	5990.50	0.52	3.07	0.44	1.10	0.37	0.24	0.70	0.71	0.73
	Y 1	5874.50	0.80	4.50	0.84	1.90	0.48	0.26	0.95	0.88	0.84
	Y 1	5878.10	0.77	5.70	0.82	1.67	0.48	0.26	0.94	0.86	0.93
	Y 1	5880.00	0.79	6.75	0.80	1.17	0.49	0.27	0.93	0.87	1.00
	Y 1	5886.50	0.83	4.95	0.85	1.69	0.49	0.26	0.96	0.90	0.87
	Y 2	5998.00	0.92	4.92	0.81	1.34	0.52	0.28	0.94	0.95	0.87
	Y 2	6000.60	0.94	5.37	1.13	1.49	0.51	0.28	1.12	0.96	0.90
	Y 2	6002.00	0.92	5.22	0.93	1.28	0.53	0.29	1.01	0.95	0.89
	Y 2	6004.28	0.76	5.33	0.67	1.34	0.51	0.30	0.86	0.86	0.90
	Y 2	6004.45	0.89	5.64	1.06	1.47	0.50	0.28	1.08	0.93	0.92
	Y 2	6004.50	0.90	5.33	0.97	1.47	0.53	0.28	1.03	0.94	0.90
	Y 3	5615.50	0.95	5.89	0.89	1.63	0.54	0.30	0.99	0.97	0.94
	Y 3	5619.00	0.91	4.39	0.98	1.56	0.50	0.28	1.04	0.95	0.83
	Y 6	6027.40	0.91	5.10	0.61	1.78	0.42	0.24	0.80	0.94	0.88
	Y 6	6028.50	0.81	3.19	1.05	1.58	0.48	0.28	1.06	0.89	0.74
	Y 6	6033.20	0.54	5.03	0.49	1.30	0.38	0.24	0.72	0.73	0.88
	Y 6	6034.00	0.75	3.90	0.58	1.24	0.42	0.24	0.79	0.85	0.80
	Y 6	6035.00	0.78	3.17	1.17	1.62	0.50	0.29	1.13	0.87	0.74
	Y 7	6099.80	0.77	6.03	0.44	0.75	0.56	0.32	0.71	0.86	0.95
	Y 8	6043.20	0.75	1.32	0.35	1.54	0.41	0.22	0.65	0.85	0.61
	Y 8	6045.00	0.57	4.76	0.27	1.37	0.33	0.19	0.58	0.74	0.86
	YJ 12	5785.40	0.85	4.11	0.55	1.77	0.37	0.20	0.76	0.91	0.81
	YJ 14	5517.50	0.96	2.26	1.05	1.84	0.49	0.27	1.07	0.97	0.67
	YJ 15	5780.00	0.92	3.56	0.61	1.84	0.38	0.22	0.79	0.95	0.77
	Y 301	5542.40	0.91	5.07	0.91	1.77	0.47	0.25	0.98	0.95	0.88
	YJ 302	5651.00	0.74	3.30	0.56	1.75	0.42	0.23	0.77	0.84	0.75
	YJ 303	5741.00	0.96	6.31	0.96	1.77	0.48	0.25	1.02	0.98	0.97
	Y 3-x17	5722.50	1.01	5.96	0.93	1.82	0.49	0.26	1.00	1.01	0.94

sample type	well	depth (m)	log (1,2,5-/1,3,6-) TMN	log (1-/9-) MP	log [1,7-/(1,3-+3,9-+2,10-+3,10-)] DMP	log (Retene/9-MP)	FL[b]	DBT[b]	DBF[b]	DBT/PHE	C_{26}/C_{28} 20S-TAS	$(C_{20-21})/(C_{20-21}+C_{26-28})$ TAS	$C_{20}/(C_{20}+C_{28}$ (20R)) TAS
Oil	Y 1	5873.00−5881.00	0.27	−0.19	−0.44	−1.08	20.40	73.50	6.10	0.07	0.14	0.16	0.33
	Y 1	5873.40−5888.10	0.08	−0.15	−0.37	−1.00	29.82	51.07	19.11	0.07	0.13	0.16	0.31
	Y 1	5873.40−5888.10	0.37	−0.17	−0.36	−1.01	42.82	49.63	7.55	0.06	0.13	0.15	0.30
	Y 3	5609.60−5619.90	−0.22	−0.17	−0.40	−0.84	48.20	44.10	7.70	0.07	0.14	0.17	0.36
	Y 301	5541.60−5552.00	0.03	−0.15	−0.43	−1.31	48.49	48.64	2.87	0.08	0.15	0.30	0.57
	YJ 302	5549.90−5655.80	0.45	−0.16	−0.36	−1.23	7.10	85.09	7.81	0.05	0.16	0.29	0.56

https://doi.org/10.1021/acsomega.4c08477
ACS Omega 2025, 10, 2735−2761

Table 5. continued

sample type	well	depth (m)	log (1,2,5-/1,3,6-) TMN	log (1-/9-) MP	log [1,7-/(1,3-+3,9-+2,10-+3,10-)] DMP	log (Retene/9-MP)	FL[b]	DBT[b]	DBF[b]	DBT/PHE	C_{26}/C_{28} 20S-TAS	$(C_{20-21})/(C_{20-21}+C_{26-28})$ TAS	$C_{20}/(C_{20}+C_{28}$ (20R)) TAS
	Y 3-x11	6021.00–6034.50	0.34	−0.15	−0.43	−1.16	29.12	69.34	1.54	0.07	0.18	0.28	0.51
	Y 3-x12	5784.20–5796.00	0.09	−0.16	−0.43	−1.23	46.59	50.93	2.47	0.08	0.16	0.26	0.52
EOM	Y 1−1	5814.43	−0.07	−0.19	−0.52	n.d.	55.58	21.62	22.80	0.10	0.11	0.23	0.50
	Y 1−1	5818.40	0.14	−0.13	−0.30	−0.93	15.84	55.51	28.65	0.07	0.15	0.16	0.39
	Y 1−1	5822.57	−0.06	−0.20	−0.53	n.d.	51.17	29.52	19.31	0.11	0.11	0.22	0.47
	Y 1−1	5839.10	0.60	−0.14	−0.09	−1.43	40.75	53.67	5.58	0.06	0.12	0.18	0.40
	YJ 1−3	5971.20	−0.06	−0.09	−0.26	−1.23	36.16	53.43	10.41	0.06	0.13	0.12	0.27
	YJ 1−3	5976.20	−0.28	−0.11	−0.36	−0.87	26.54	38.86	34.60	0.06	0.16	0.18	0.36
	YJ 1−3	5978.50	0.03	−0.09	−0.32	−0.93	21.05	58.27	20.68	0.08	0.16	0.14	0.33
	YJ 1−3	5982.15	−0.11	−0.08	−0.25	−1.64	21.24	22.99	55.77	0.05	0.22	0.12	0.24
	YJ 1−3	5987.85	0.41	−0.09	−0.05	−1.22	14.28	54.17	31.55	0.06	0.14	0.15	0.37
	YJ 1−3	5988.90	−0.11	−0.08	−0.26	−1.22	31.90	54.94	13.16	0.06	0.16	0.14	0.31
	YJ 1−3	5990.50	0.25	−0.09	−0.08	−1.30	14.23	34.64	51.12	0.05	0.13	0.16	0.36
	Y 1	5874.50	0.30	−0.14	−0.36	−1.87	2.93	90.89	6.19	0.25	0.12	0.15	0.30
	Y 1	5878.10	0.14	−0.15	−0.39	−0.94	16.01	58.24	25.75	0.04	0.14	0.15	0.31
	Y 1	5880.00	0.00	−0.13	−0.35	−0.98	3.36	55.03	41.61	0.04	0.14	0.15	0.32
	Y 1	5886.50	0.31	−0.14	−0.37	−0.93	16.89	68.00	15.12	0.04	0.14	0.16	0.33
	Y 2	5998.00	0.16	−0.07	−0.31	−0.72	14.48	31.09	54.43	0.04	0.14	0.12	0.25
	Y 2	6000.60	−0.31	−0.13	−0.40	−1.24	5.25	92.95	1.79	0.04	0.13	0.21	0.38
	Y 2	6002.00	−0.07	−0.12	−0.40	−1.13	14.87	56.66	28.47	0.05	0.17	0.16	0.32
	Y 2	6004.28	−0.03	−0.12	−0.33	−1.08	13.71	43.38	42.91	0.07	0.39	0.32	0.60
	Y 2	6004.45	−0.21	−0.14	−0.40	−1.46	6.99	89.84	3.17	0.05	0.17	0.43	0.66
	Y 2	6004.50	−0.04	−0.14	−0.41	−1.08	13.93	66.81	19.25	0.06	0.17	0.15	0.34
	Y 3	5615.50	−0.18	−0.13	−0.40	−1.33	17.86	53.40	28.74	0.06	0.21	0.23	0.48
	Y 3	5619.00	0.31	−0.12	−0.34	−1.34	7.09	91.26	1.65	0.05	0.13	0.15	0.33
	Y 6	6027.40	0.08	−0.15	−0.32	−0.77	28.49	66.51	5.00	0.05	0.21	0.09	0.19
	Y 6	6028.50	−0.37	−0.16	−0.35	−1.43	9.66	86.31	4.02	0.05	0.11	0.14	0.31
	Y 6	6033.20	0.20	−0.14	−0.18	−1.17	10.07	34.43	55.50	0.05	0.15	0.16	0.38
	Y 6	6034.00	0.06	−0.07	−0.24	−0.56	12.55	45.26	42.19	0.05	0.25	0.09	0.19
	Y 6	6035.00	−0.39	−0.11	−0.36	−1.20	8.02	88.40	3.58	0.05	0.13	0.12	0.25
	Y 7	6099.80	0.05	0.00	−0.22	−0.82	11.73	40.76	47.51	0.05	0.32	0.33	0.61
	Y 8	6043.20	0.22	−0.35	n.d.	n.d.	18.20	18.07	63.73	0.06	0.14	0.07	0.19
	Y 8	6045.00	0.30	−0.24	−0.45	−1.45	6.71	72.54	20.74	0.09	0.31	0.11	0.28
	YJ 12	5785.40	0.39	−0.21	−0.36	−1.22	38.71	57.26	4.02	0.07	0.14	0.22	0.45
	YJ 14	5517.50	−0.46	−0.13	−0.43	−0.97	32.62	48.44	18.94	0.06	0.34	0.14	0.31
	YJ 15	5780.00	0.21	−0.16	−0.27	−1.46	21.73	72.28	5.99	0.06	0.13	0.15	0.35
	Y 301	5542.40	0.10	−0.15	−0.46	−1.16	26.36	69.76	3.88	0.06	0.13	0.19	0.42
	YJ 302	5651.00	0.50	−0.15	−0.17	−1.45	43.22	50.63	6.14	0.05	0.14	0.24	0.51
	YJ 303	5741.00	0.10	−0.16	−0.45	−1.19	14.78	82.70	2.52	0.07	0.13	0.21	0.44
	Y 3-x17	5722.50	0.00	−0.16	−0.41	−1.20	18.03	79.53	2.45	0.07	0.17	0.16	0.37

[a]TMN, trimethylnaphthalene; MP, methylphenanthrene; DMP, dimethylphenanthrene; TAS, triaromatic steroid; TNR-2 = (2,3,6- + 1,3,7-TMN)/(1,4,6- + 1,3,5- + 1,3,6-TMN); MDR = 4-MDBT/1-MDBT; MPI-1 = 1.5 × (3- + 2-MP)/(P + 9- + 1-MP); MNR = 2-MN/1-MN; F1 = (3- + 2-MP)/(2- + 3- + 1- + 9-MP); F2 = (2-MP)/(2- + 3- + 1- + 9-MP); VR_{MPI-1} = 0.60 × MPI-1 + 0.40;VR_{TNR-2} = 0.60 × TNR-2 + 0.40; VR_{MDR} = 0.073 × MDR + 0.51; FL, fluorene; DBT, dibenzothiophene; DBF, dibenzofurane; FL (%) = 100 × FL/(FL + DBT + DBF), DBT (%) and DBF (%) obtained via similar calculation). [b]Normalized concentrations of FL, DBT, and DBF (%).

a complete homologous series of 25-norhopanes indicates severe biodegradation with ranks >4.[27] Actually, 25-norhopanes can appear in only slightly biodegraded or nonbiodegraded oils that are predominated by acyclic isoprenoids and *n*-alkanes in saturated hydrocarbons. This phenomenon is generally interpreted as oils are mixtures of biodegraded with non-degraded oil during accumulation in reservoirs.[27] Additionally, 25-norhopanes can also be observed in sediments where OM is immature and *n*-alkanes predominate in saturated hydrocarbon fraction.[37] This complexity suggests that the 25-norhopanes should be used with caution when assessing biodegradation scales. Combined with the above-mentioned evidence, the OM degradation can be assessed at a scale of 3 to 4 for the most studied samples. Although the crude oil in the study area is subject to biodegradation, this has a limited influence on the parameters selected for oil-source comparison.

5.5. Potential Origins. The Jurassic source rocks typically feature low Tri and Gamm abundances as well as few concentrations of β-carotan with predominant C_{29} steranes in aliphatic hydrocarbons (e.g., refs 22,100).

Regarding aromatic compounds, the Jurassic source rocks are characterized by the dominance of naphthalene and its alkylated

https://doi.org/10.1021/acsomega.4c08477
ACS Omega 2025, 10, 2735−2761

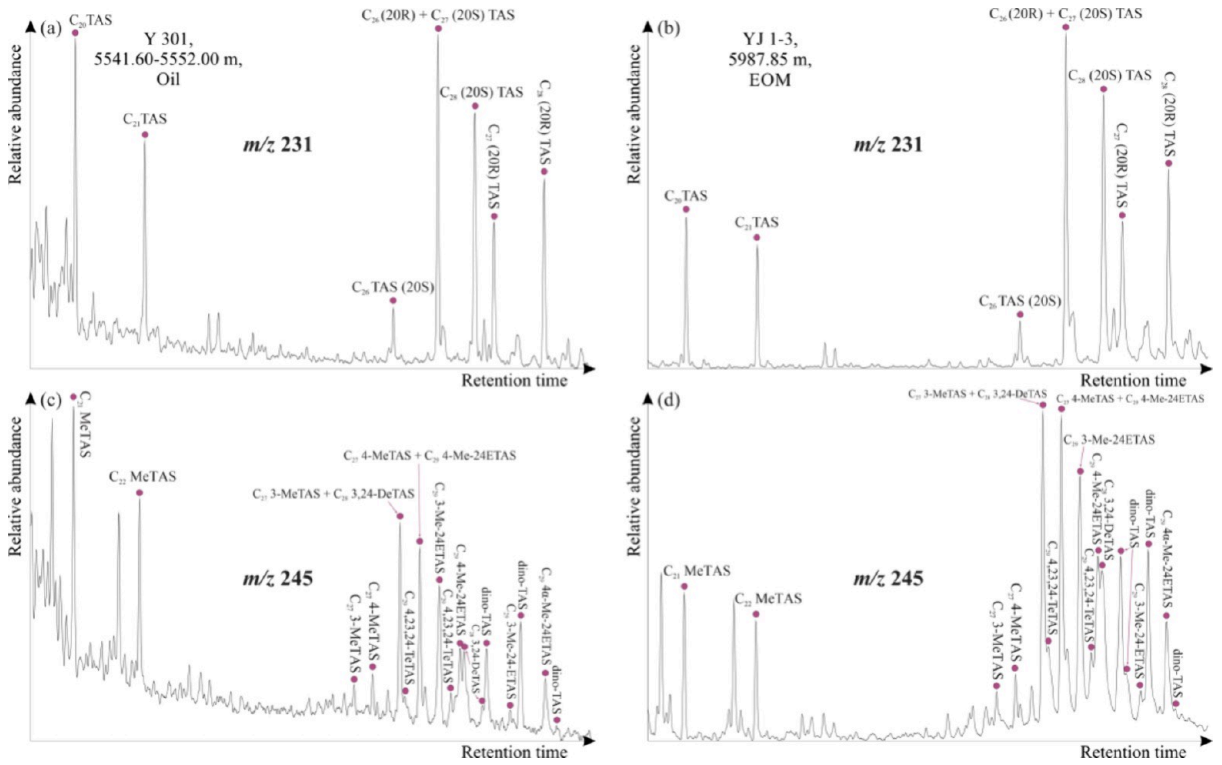

Figure 8. Representative mass chromatograms of (a, b) the triaromatic steroids (m/z 231) and of (c, d) the methyl-triaromatic steroids and dino-TAS (m/z 245) (figures on the left represent the oil sample from the Y 301 well, and those on the right represent the EOM sample from the YJ 1−3 well). Notes: MeTAS = methyltriaromatic steroids; DeTAS, dimethyltriaromatic steroids; TeTAS, trimethyltriaromatic steroids; Me-24ETAS, methyl-24-ethyltriaromatic steroids; dino-TAS, C_{29} 4α,23,24-trimethyltriaromatic steroids.

Table 6. Stable Organic Carbon Isotope Compositions of the Oil and EOM Samples from the Qigu Formation in the Yongjin Area of the Junggar Basin, China

			before fractionation	components of after fractionation			
sample type	well	depth (m)	$\delta^{13}C_{oil/EOM}$ (‰PDB)	$\delta^{13}C_{Sat}$ (‰PDB)	$\delta^{13}C_{Aro}$ (‰PDB)	$\delta^{13}C_{Res}$ (‰PDB)	$\delta^{13}C_{Asp}$ (‰PDB)
Oil	Y 1	5873.40−5888.10	−30.2	−31.1	−28.8	−29.2	−29.6
	Y 1	5873.40−5888.10	−30.1	−31.0	−29.5	−29.0	−29.7
	Y 1	5873.40−5888.10	−30.7	−31.1	−28.9	−29.0	−29.9
	Y 1-p1	6152.00−6170.60	−29.5	−30.2	−29.2	−29.4	−30.1
	Y 3	5609.60−5619.90	−30.0	−30.4	−28.7	−28.4	−29.6
	Y 3	5609.60−5619.90	−30.1	−31.0	−29.6	−28.9	−29.7
	Y 3-cp1	5775.85−6110.80	−29.7	−29.7	−28.5	−28.9	−29.5
	Y 6	5858.40−5869.70	−31.4	−31.9	−30.9	−30.0	−30.8
	Y 6	5858.40−5869.70	−31.8	−32.2	−31.6	−30.2	−31.0
	Y 9	5914.00−5916.00	−30.2	−30.5	−29.3	−29.1	−30.0
	YJ 303	5738.20−5752.80	−28.4	−29.8	−28.2	−29.1	−29.5
	YJ 304C	6434.00−6443.20	−29.2	−30.1	−28.8	−29.2	−29.7
EOM	Y 1	5874.50	−30.1	−31.1	−29.7	−29.3	−28.6
	Y 1	5878.10	−30.2	−31.0	−29.6	−29.0	−28.8
	Y 1	5880.00	−30.3	−30.9	−29.2	−28.7	−28.8
	Y 1	5886.50	−30.4	−31.1	−29.5	−28.3	−28.1
	Y 2	5998.00	−28.9	−29.8	−27.8	−27.6	−28.4
	Y 2	6002.00	−29.3	−29.8	−28.4	−27.7	−28.2
	Y 2	6004.50	−29.6	−29.9	−28.3	−27.9	−29.1
	Y 6	6034.00	−31.3	−31.8	−30.7	−29.4	−30.8
	Y 8	6043.20	−29.9	−31.9	−29.5	−29.8	−29.0
	Y 8	6045.00	−30.3	−30.5	−29.8	−30.1	−29.5

analogues, as well as abundant polycyclic compounds,[20] alongside higher abundances of C_{26} 20S TAS.[22] These characteristics markedly differ from those of the oil and EOM samples from the Qigu reservoirs. The $\delta^{13}C$ values for the studied oil and EOM samples also rule out the possibility that the oils were sourced from the Jurassic source rocks.

Both the Fengcheng and lower Wuerhe source rocks were deposited in alkaline paleolakes, developing similar composi-

https://doi.org/10.1021/acsomega.4c08477
ACS Omega 2025, 10, 2735−2761

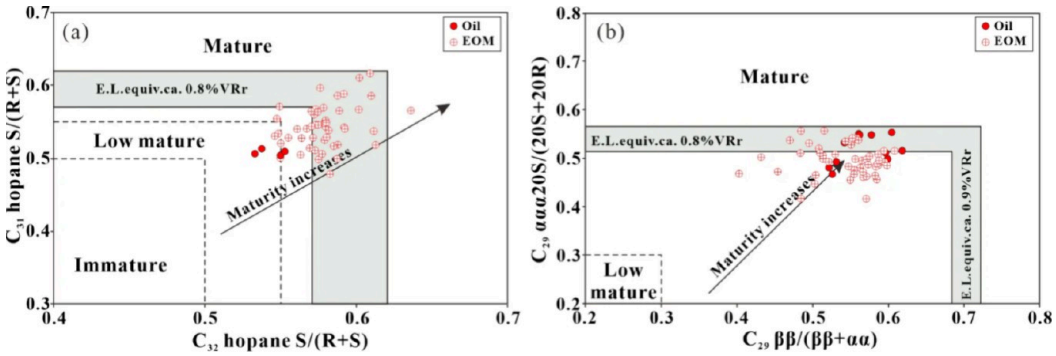

Figure 9. Molecular thermal maturity indicators of the oil and EOM samples from the Qigu Formation in the Yongjin area, Junggar Basin, China. (a) C_{31} homohopane 22S/(22S + 22R) vs C_{32} homohopane 22S/(22S + 22R), and (b) C_{29} $\alpha\alpha\alpha$ 20S/(20S + 20R) vs C_{29} $\beta\beta/(\beta\beta + \alpha\alpha)$.

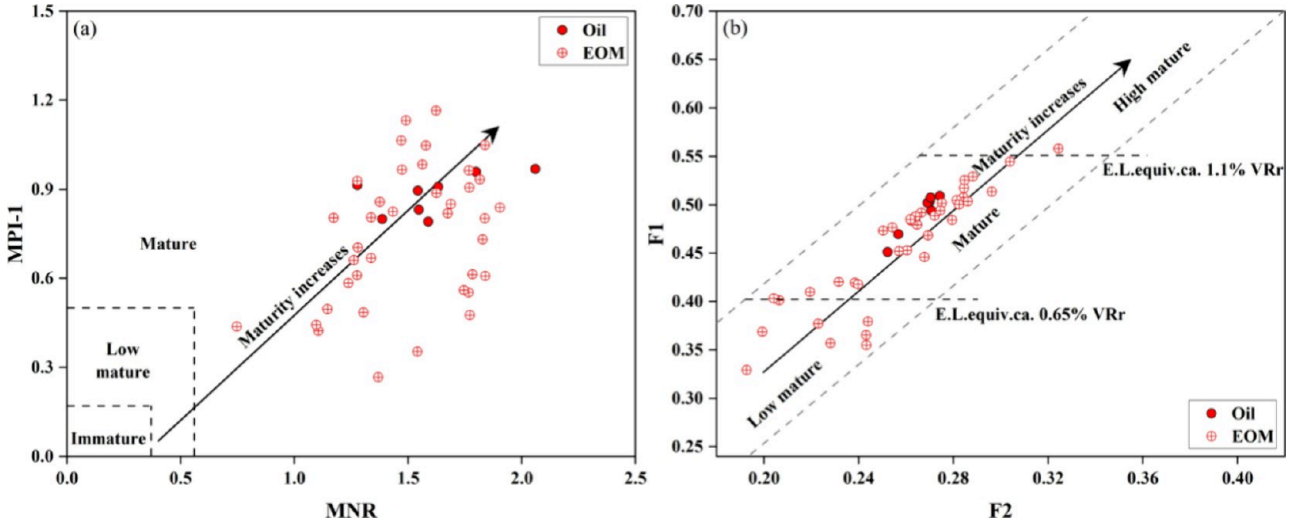

Figure 10. Plots of (a) methylnaphthalene ratio vs methylphenanthrene index 1 (modified after Wang et al.[31]) and (b) F1 vs F2 indicating the thermal maturity for the oil and EOM samples from the Qigu Formation in the Yongjin area of the Junggar Basin, China.

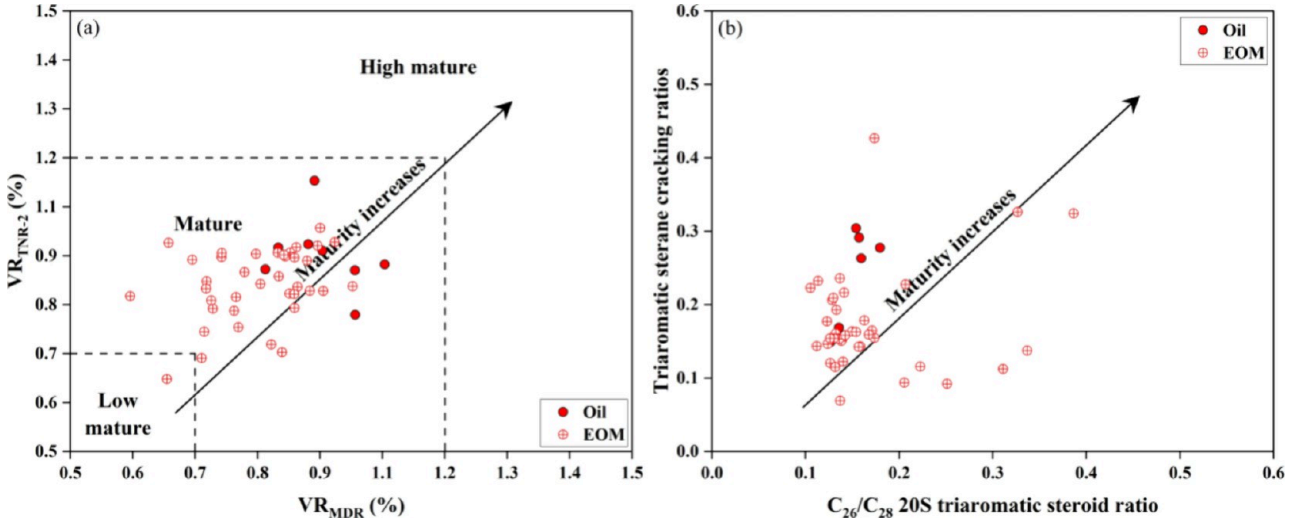

Figure 11. Pltos of (a) VR_{TNR-2} vs VR_{MDR} and (b) triaromatic sterane cracking ratios vs C_{26}/C_{28} 20S triaromatic steroid ratio, showing thermal maturity for the oil and EOM samples from the Qigu Formation in the Yongjin area of the Junggar Basin, China.

tions and characteristics in organic geochemistry (Figure 6; Table 3). Nevertheless, there are still some discernible differences between them. Due to the high thermal maturity of the source rocks from the ZS 101 well, most organic geochemical parameters are invalid, so published data with appropriate thermal maturity used for oil and source correlation were collected. The ratios of Pr/*n*-C_{17} of <0.5 and Ph/*n*-C_{18} of <0.5 can be observed in both the Jurassic Qigu and lower Wuerhe samples but not in the Fengcheng samples (Figure 20a). In addition, the Fengcheng samples generally have lower Pr/Ph

https://doi.org/10.1021/acsomega.4c08477
ACS Omega 2025, 10, 2735−2761

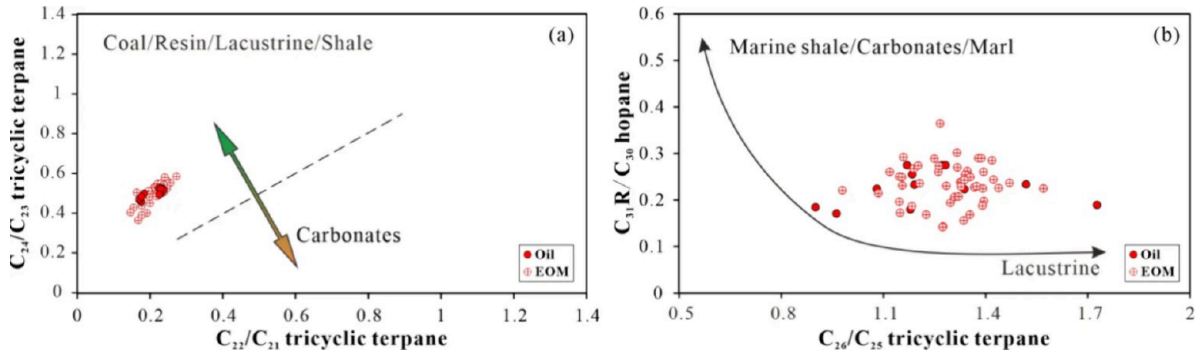

Figure 12. Plots of (a) C_{22}/C_{21} vs C_{24}/C_{23} tricyclic terpane and (b) C_{26}/C_{25} tricyclic terpane vs C_{31} R/C_{30} hopane for the oil and EOM samples from the Qigu Formation in the Yongjin area of the Junggar Basin, China. (modified after Qiao et al.,[36]).

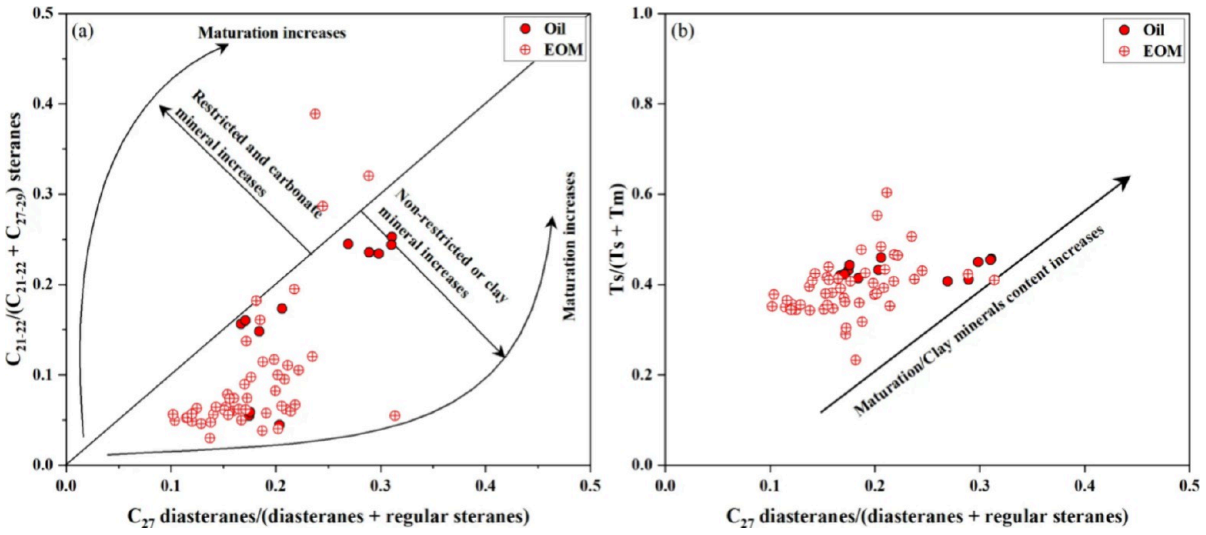

Figure 13. Plots of (a) $C_{21-22}/(C_{21-22} + C_{27-29})$ steranes vs C_{27} diasteranes/(diasteranes + regular steranes) and (b) Ts/(Ts + Tm) vs C_{27} diasteranes/(diasteranes + regular steranes) for the oil and EOM samples from the Qigu Formation in the Yongjin area of the Junggar Basin, China.

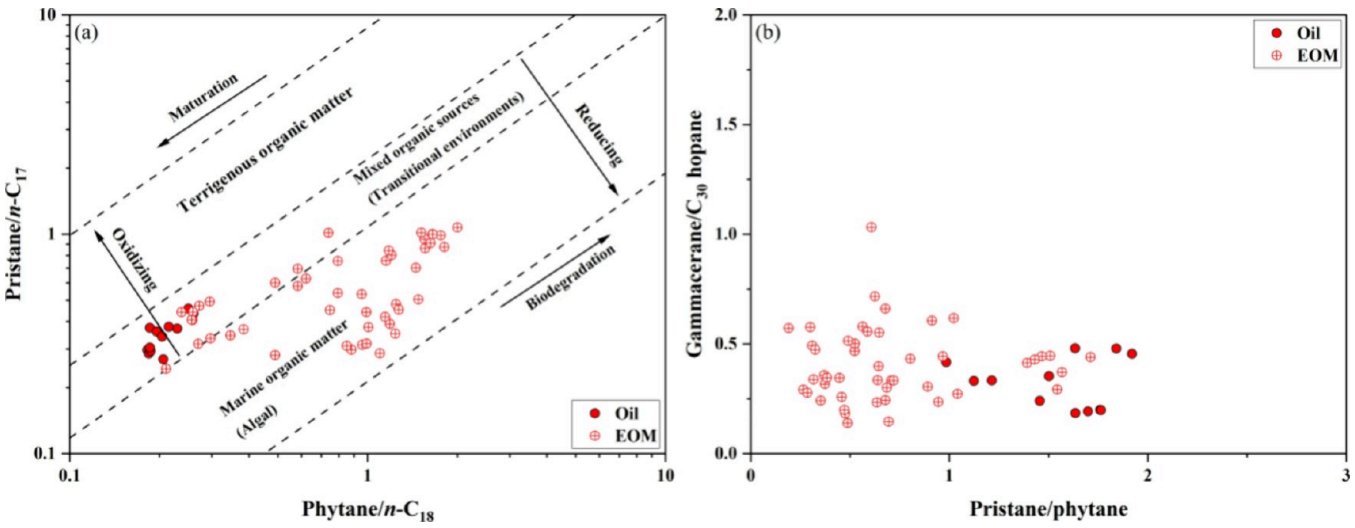

Figure 14. Plots of (a) Pr/n-C_{17} vs Ph/n-C_{18} and (b) gammacerane/C_{30} hopane vs Pr/Ph for the oil and EOM samples from the Qigu Formation in the Yongjin area of the Junggar Basin, China.

values than the lower Wuerhe samples as well as the studied EOM and oil samples, which aligns with observations in other studies (e.g., ref 101) and in the source rocks of the ZS 101 well (Figure 18). Hopanoids/steranes ratios are also completely different between the Fengcheng Fm. (<1.0) and the lower Wuerhe Fm. (>1.0),[101] which indicates the studied oils and EOMs are more likely to have been generated from the lower Wuerhe Fm. (Figure 21a). Moreover, the lower Wuerhe source rocks and the studied oil and EOM samples are characterized by higher C_{20}/C_{23} Tri ratios, while the C_{20}/C_{23} Tri ratios are lower

https://doi.org/10.1021/acsomega.4c08477
ACS Omega 2025, 10, 2735−2761

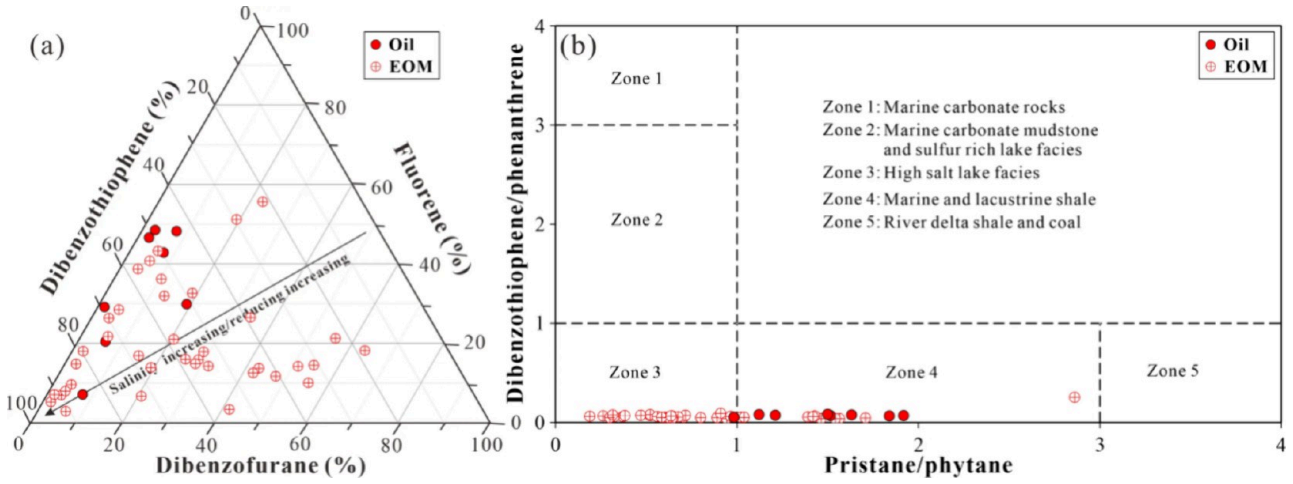

Figure 15. (a) Relative concentrations of fluorene (FL), dibenzofuran (DBF), and dibenzothiophene (DBT) as well as (b) dibenzothiophene/phenanthrene ratio vs Pr/Ph ratio indicating paleosalinity conditions and depositional environment for the oil and EOM samples from the Qigu Formation in the Yongjin area of the Junggar Basin, China.

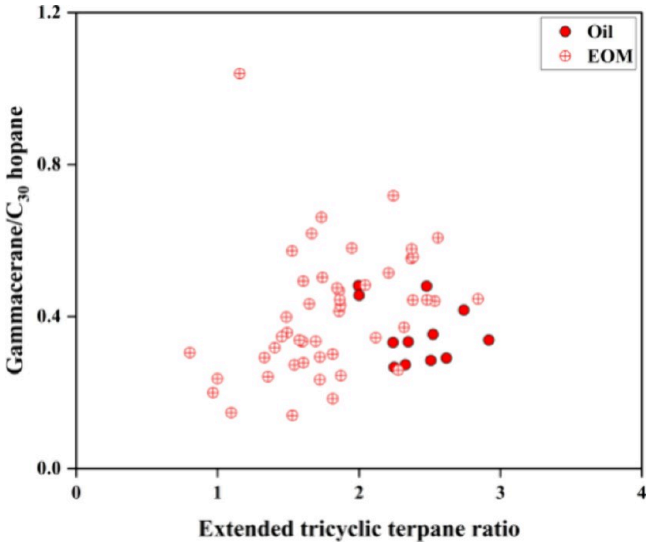

Figure 16. Extended tricyclic terpane vs gammacerane/C_{30} hopane indicating paleosalinity conditions for the oil and EOM samples from the Qigu Formation in the Yongjin area of the Junggar Basin, China.

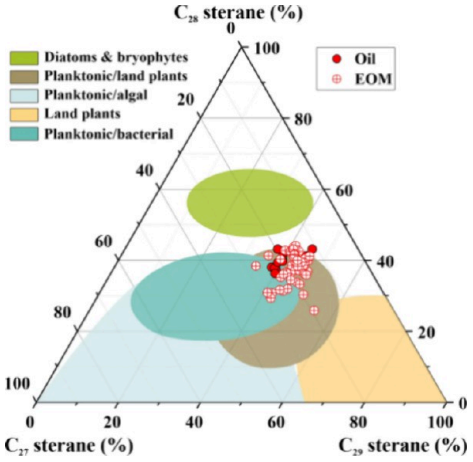

Figure 17. Ternary diagram showing the distribution of C_{27}, C_{28} and C_{29} regular steranes for the oil and EOM samples from the Qigu Formation in the Yongjin area of the Junggar Basin, China (modified after Huang and Meinschein[66]).

in the Fengcheng source rocks (Figure 21a). Furthermore, the β-carotane/n-C_{max} ratios in the Fengcheng Fm. are generally greater than 0.1, but some of them are smaller than 0.1 for the samples from the lower Wuerhe Fm. as well as the studied EOM and oil samples (Figure 21b). Steranes can also be used to distinguish the source rocks from the lower Wuerhe Fm. and Fengcheng Fm. and used to correlate oil and source. The too low C_{28} steranes concentrations (<10%) in the normalized concentrations of C_{27}, C_{28}, and C_{29} steranes can be observed only in some Fengcheng source rocks (Figure 22), which contrast markedly with the studied oil and EOM samples, and the C_{27}/C_{29} sterane ratios of >0.4 are more abundant in the lower Wuerhe source rocks and the studied oils and EOMs (Figure 21b).

In summary, the oil and EOM samples investigated herein exhibit characteristics more closely aligned with the OM in the lower Wuerhe source rocks. Although the geochemical characteristics of the source rocks from the lower Wuerhe and Fengcheng Fm. exhibit some different trends based on the data analysis (more than 1000 data), there are overlapping geochemical characteristics in the source rocks of these two formations, so the possibility that the Jurassic oils generated from the Fengcheng Fm. cannot be completely ruled out in the Yongjin area.

6. CONCLUSIONS

The geochemical investigation involved detailed molecular and isotope characteristics analyses on 14 oils, 49 extractable organic matter (EOM) from sandstones, and 13 source rock samples was performed on a major, yet understudied, oil field trapped in the Upper Jurassic Qigu Formation (Fm.) in the Yongjin area. The study revealed that a singular oil group is trapped in the Qigu Fm. in the studied area, as evidenced by the similar geochemical characteristics observed in both the oil and EOM samples. The thermal maturity of the organic matter (OM) is mainly in the oil window, and the degradation scales of the OM range between 3 and 4 for the studied oils and EOM samples. These oil and EOM samples are typically generated from lacustrine source rocks with minimal variations in the lithology. Additionally, the related source rocks were likely deposited in a

https://doi.org/10.1021/acsomega.4c08477
ACS Omega 2025, 10, 2735−2761

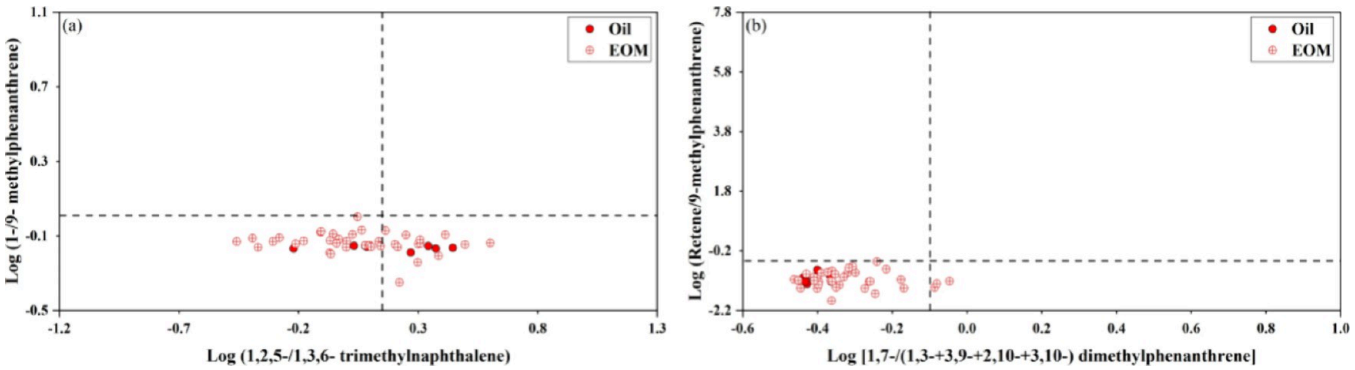

Figure 18. Plots of (a) log (1,2,5-/1,3,6-trimethylnaphthalene) vs log (1-/9-methyphenanthrene), and (b) log [1,7-/(1,3- + 3,9- + 2,0- + 3,10-) dimethylphenanthrene] vs log (Retene/9-dimethylphenanthrene) for the oil and EOM samples from the Qigu Formation in the Yongjin area of the Junggar Basin, China.

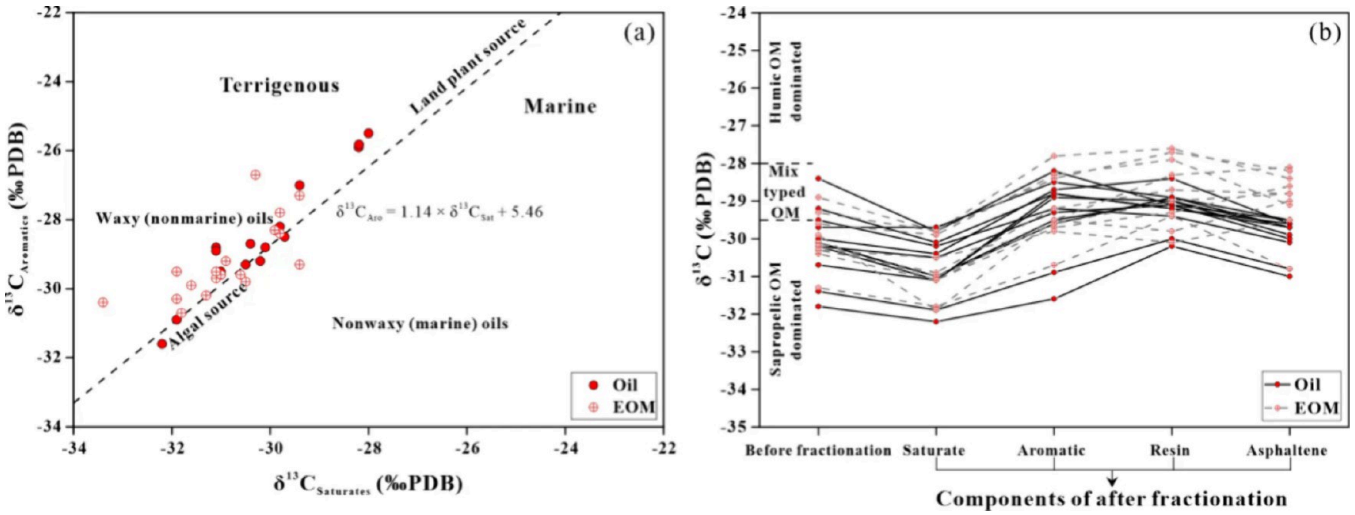

Figure 19. (a) $\delta^{13}C_{Saturates}$ vs $\delta^{13}C_{Aromatics}$ as well as (b) stable organic carbon isotope compositions of the samples before fractionation and components after fractionation for the oil and EOM samples from the Qigu Formation in the Yongjin area of the Junggar Basin, China. The dashed line in (a) is the best-fit separation for waxy and nonwaxy hydrocarbons.

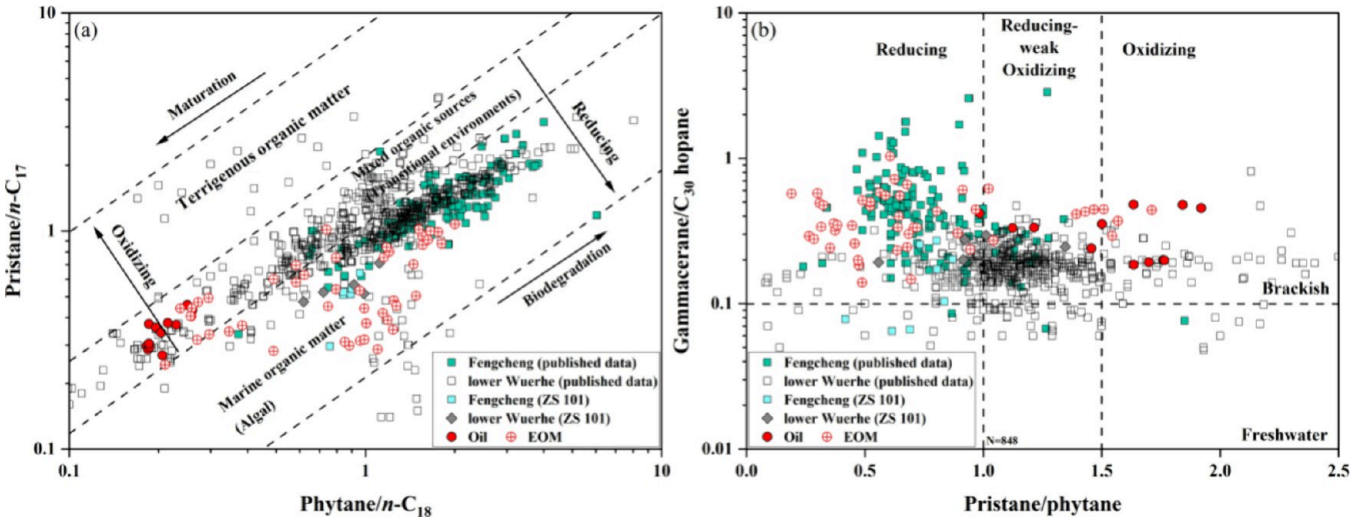

Figure 20. Plots of (a) Pr/n-C_{17} vs Ph/n-C_{18} and (b) gammacerane/C_{30} hopane vs Pr/Ph showing paleoredox conditions for the oil and EOM samples from the Qigu Formation and source rocks from Fengcheng and lower Wuerhe/Lucaogou/Pingdiquan Formation covering the whole Junggar Basin. Note: published data from publication.[17,100−114]

hypersaline environment. The origins of OM are mainly from abundant bacteria and algae (e.g., methanogens, cyanobacteria, and dinoflagellates), with little contribution from terrestrial higher plants. A stark contrast in geochemical characteristics was

https://doi.org/10.1021/acsomega.4c08477
ACS Omega 2025, 10, 2735−2761

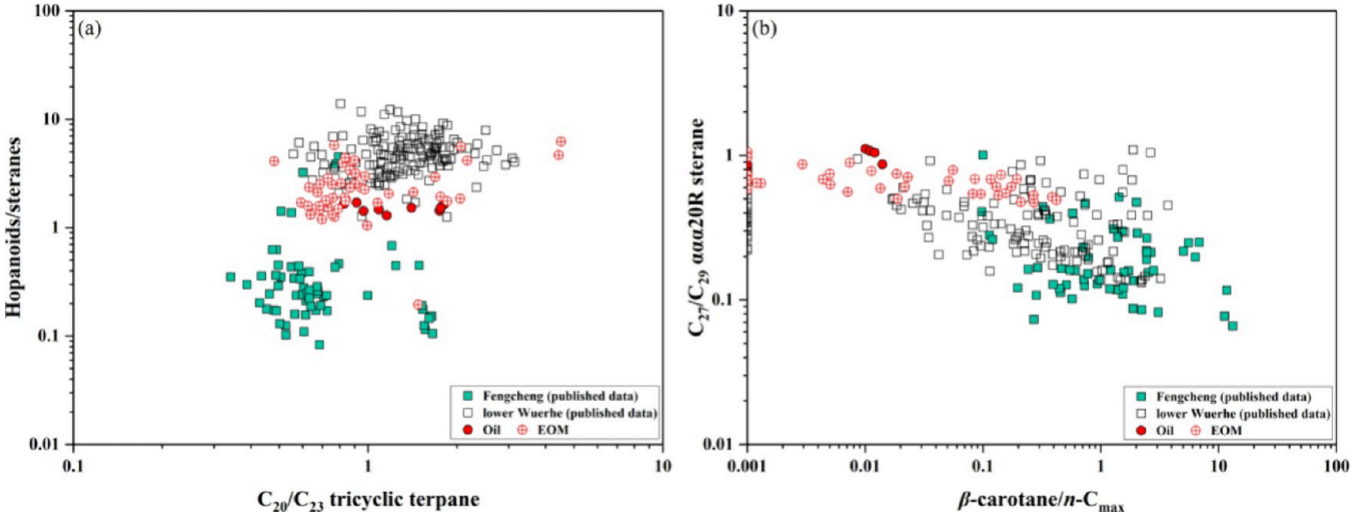

Figure 21. Plots of (a) hopanes/steranes vs C_{20}/C_{23} tricyclic terpane and (b) β-carotane/n-C_{max} vs C_{27}/C_{29} $\alpha\alpha\alpha$ 20R sterane for the oil and EOM samples from the Qigu Formation and source rocks from the Fengcheng and lower Wuerhe/Lucaogou/Pingdiquan Formation covering the whole Junggar Basin). Note: published data from publication.[101]

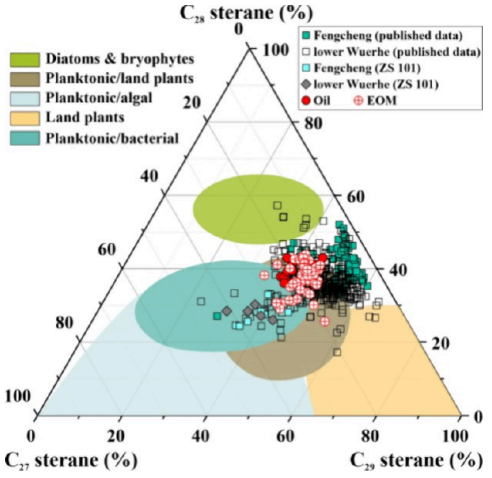

Figure 22. Ternary diagram showing the distribution of C_{27}, C_{28} and C_{29} regular steranes for the oil and EOM samples from the Qigu Formation and source rocks from Fengcheng and lower Wuerhe/Lucaogou/Pingdiquan Formation covering the whole Junggar Basin (modified after Huang and Meinschein[66]). Note: published data from the same references are given in Figure 20.

observed between the Jurassic Badaowan coal-bearing source rocks and the Permian source rocks, making it highly improbable that the Jurassic Qigu oils originated from the Jurassic source rocks. The Permian strata in the Yongjin region are buried more than 7000 m, so the OM in the Permian source rocks provides limited organic geochemical characteristics because of the high thermal maturity stage of the OM. Although there are some similarities in the OM origins and depositional environments of the Fengcheng and lower Wuerhe source rocks, subtle compositional differences, as indicated by the Permian source rocks in this study and over 1000 published data, suggest that the oils trapped in the Qigu reservoirs are most likely generated from the lower Wuerhe source rocks.

■ ASSOCIATED CONTENT

Data Availability Statement

Data are contained within the article.

■ AUTHOR INFORMATION

Corresponding Author

Jinqi Qiao − *Key Laboratory of Shale Gas Exploration, Ministry of Natural Resources and College of Geoscience, China University of Petroleum, Beijing 102249, China;* orcid.org/0000-0001-6240-6389; Email: jinqi.qiao@cup.edu.cn

Authors

Yansheng Qu − *Key Laboratory of Shale Gas Exploration, Ministry of Natural Resources and College of Geoscience, China University of Petroleum, Beijing 102249, China*

Ningning Zhong − *Key Laboratory of Shale Gas Exploration, Ministry of Natural Resources and College of Geoscience, China University of Petroleum, Beijing 102249, China*

Wei Li − *Key Laboratory of Shale Gas Exploration, Ministry of Natural Resources and College of Geoscience, China University of Petroleum, Beijing 102249, China; PetroChina Changqing Oilfield Company, Xi'an 710000, China*

Guanlong Zhang − *Exploration and Development Research Institute of Shengli Oilfield, SINOPEC, Dongying, Shandong 257061, China*

Hongzhou Yu − *Exploration and Development Research Institute of Shengli Oilfield, SINOPEC, Dongying, Shandong 257061, China*

Gui Wang − *China National Nuclear Corporation, Urumqi, Xinjiang 830011, China*

Fangchao Yan − *CNNC Geological Exploration Group Co., Ltd., Beijing 100013, China*

Complete contact information is available at: https://pubs.acs.org/10.1021/acsomega.4c08477

Notes

The authors declare no competing financial interest.

■ ACKNOWLEDGMENTS

The authors gratefully acknowledge the financial support from the Science Foundation of China University of Petroleum, Beijing under project number ZX20220074 and the "Assume leadership" project of the Natural Uranium Industry Technology Innovation Consortium, "Key factors and metallogenic

https://doi.org/10.1021/acsomega.4c08477
ACS Omega 2025, 10, 2735−2761

mechanism of red uranium formation in northern sedimentary basin" under project number 202301.

REFERENCES

(1) Han, S.; Xie, L.; Du, X.; Xiang, C.; Huang, J.; Tang, Z.; Wang, C.; Horsfield, B.; Mahlstedt, N. Insights into organic metagenesis using Raman spectroscopy and high resolution mass spectrometry: A case study of the Shahezi formation, deep Songliao basin China. *Int. J. Coal Geol.* **2023**, *265*, No. 104153.

(2) Hu, Y.; Cai, C.; Li, Y.; Liu, D.; Wei, T.; Wang, D.; Jiang, L.; Ma, R.; Shi, S.; Immenhauser, A. Sedimentary and diagenetic archive of a deeply buried, upper Ediacaran microbialite reservoir, southwestern China. *AAPG Bull.* **2023**, *107* (3), 387−412.

(3) Xu, K.; Yang, H.; Zhang, H.; Ju, W.; Li, C.; Fang, L.; Wang, Z.; Wang, H.; Yuan, F.; Zhao, B.; Zhang, W.; Liang, J. Fracture effectiveness evaluation in ultra-deep reservoirs based on geomechanical method, Kuqa Depression, Tarim Basin NW China. *J. Pet. Sci. Eng.* **2022**, *215*, No. 110604.

(4) Su, J.; Wang, X.; Yang, H.; Yu, F.; Li, Y.; Ma, S.; Wei, C.; Weng, N.; Yang, Y. Hydrothermal alteration and hydrocarbon accumulations in ultra-deep carbonate reservoirs along a strike-slip fault system, Tarim Basin NW China. *J. Pet. Sci. Eng.* **2021**, *203*, No. 108605.

(5) Dyman, T. S.; Crovelli, R. A.; Bartberger, C. E.; Takahashi, K. I. Worldwide Estimates of Deep Natural Gas Resources Based on the U. S. Geological Survey World Petroleum Assessment 2000. *Nat. Resour. Res.* **2002**, *11* (3), 207−218.

(6) Zhang, S.; Huang, H.; Su, J.; Liu, M. Ultra-deep liquid hydrocarbon exploration potential in cratonic region of the Tarim Basin inferred from gas condensate genesis. *Fuel* **2015**, *160*, 583−595.

(7) Xu, Z.; Sun, J. S.; Liu, J. P.; Lv, K. H.; Dong, X. D.; Wang, Z. L.; Zhang, T. F.; Sun, Y. W.; Dai, Z. W. Development and performance evaluation of high temperature resistant strong adsorption rigid blocking agent. *Pet. Sci.* **2024**, *21* (4), 2650−2662.

(8) Zhang, Q.; Littke, R.; Zieger, L.; Shabani, M.; Tang, X.; Zhang, J. Ediacaran, Cambrian, Ordovician, Silurian and Permian shales of the Upper Yangtze Platform, South China: Deposition, thermal maturity and shale gas potential. *Int. J. Coal Geol.* **2019**, *216*, No. 103281.

(9) Zhu, G.; Milkov, A. V.; Li, J.; Xue, N.; Chen, Y.; Hu, J.; Li, T.; Zhang, Z.; Chen, Z. Deepest oil in Asia: Characteristics of petroleum system in the Tarim basin China. *J. Pet. Sci. Eng.* **2021**, *199*, No. 108246.

(10) Jiang, F.; Chen, X.; Wang, P.; Shao, X.; Yang, H. Genesis and Accumulation of Paleo-Oil Reservoir in Dabei Area, Kuqa Depression, Northwest China: Implications for Tight-Gas Accumulation. *J. Earth Sci.* **2024**, *35* (2), 655−665.

(11) Yang, B.; Wu, H.; Peng, M. Deep Sandstone Reservoir Characteristics and Pore Structure Classification Based on Fractal Theory: A Case Study of the Bayingobi Formation in Guaizihu Sag Yin'e Basin. *ACS Omega* **2024**, *9* (15), 16976−16991.

(12) Wang, T. G.; He, F.; Wang, C.; Zhang, W.; Wang, J. Oil filling history of the Ordovician oil reservoir in the major part of the Tahe Oilfield, Tarim Basin NW China. *Org. Geochem.* **2008**, *39* (11), 1637−1646.

(13) Huang, H.; Zhang, S.; Su, J. Palaeozoic oil−source correlation in the Tarim Basin NW China: A review. *Org. Geochem.* **2016**, *94*, 32−46.

(14) Chen, Z.; Xie, J.; Qiao, R.; Qiu, L.; Yang, Y.; Wen, Z.; Xu, Y.; Tang, Y. Geochemistry and accumulation of Jurassic oil in the central Junggar Basin, western China. *J. Pet. Sci. Eng.* **2022**, *216*, No. 110855.

(15) Chen, J.; Deng, C.; Liang, D.; Wang, X.; Zhong, N.; Song, F.; Shi, X.; Jin, T.; Xiang, S. Mixed oils derived from multiple source rocks in the Cainan oilfield, Junggar Basin, Northwest China. Part II: artificial mixing experiments on typical crude oils and quantitative oil-source correlation. *Org. Geochem.* **2003**, *34* (7), 911−930.

(16) Wang, D. Y.; Li, M. J.; Zhou, Y.; Yang, L.; Yang, Y. F.; Li, E. T.; Jin, J.; Zou, X. L.; Xu, B. D. Petroleum geochemistry and origin of shallow-buried saline lacustrine oils in the slope zone of the Mahu sag, Junggar Basin NW China. *Pet. Sci.* **2023**, *20* (6), 3363−3378.

(17) Luo, Q.; Gong, L.; Qu, Y.; Zhang, K.; Zhang, G.; Wang, S. The tight oil potential of the Lucaogou Formation from the southern Junggar Basin China. *Fuel* **2018**, *234*, 858−871.

(18) Qiao, J.; Luo, Q.; Zhang, K.; Zhang, G.; Duan, J.; Wang, D.; Yu, H.; Wang, S.; Qu, Y.; Kopaevich, L. Geochemistry and organic petrography of the Middle Permian Lucaogou alkaline lacustrine oil shale in the southern Junggar Basin, China: Implications for formation conditions and organic matter accumulation. *Int. J. Coal Geol.* **2023**, *268*, No. 104198.

(19) Qiao, J.; Li, H.; Luo, Q.; Liu, L.; Wang, D.; Shang, X.; Zhang, T., Development conditions and factors controlling the formation of the Permian Pingdiquan source rocks in the Wucaiwan Sag, Junggar Basin, China: a comprehensively elemental, biomarker and isotopic perspective. *J. Earth Sci.* **2025**. in Press.

(20) Qiao, J.; Luo, Q.; Zhang, Y.; Wang, D.; Cui, H.; Shang, X.; Liu, L.; Zhang, T. Formation conditions and enrichment mechanisms of the Jurassic lacustrine organic-rich shale in the East Fukang Sag, Junggar Basin, NW China: A reassessment based on organic geochemistry. *Front. Earth Sci.* **2023**, *11*, No. 1086827.

(21) Li, B.; He, D.; Li, M.; Chen, L.; Yan, K.; Tang, Y. Biomarkers and Carbon Isotope of Monomer Hydrocarbon in Application for Oil−Source Correlation and Migration in the Moxizhuang−Yongjin Block, Junggar Basin. *NW China. ACS Omega* **2022**, *7* (50), 47317−47329.

(22) Qiao, J.; Littke, R.; Grohmann, S.; Zhang, C.; Jiang, Z.; Strauss, H.; Zieger, L. Climatic and environmental conditions during the Pleistocene in the Central Qaidam Basin, NE Tibetan Plateau: Evidence from GDGTs, stable isotopes and major and trace elements of the Qigequan Formation. *Int. J. Coal Geol.* **2022**, *254*, No. 103958.

(23) Luo, Q.; Goodarzi, F.; Zhong, N.; Qiu, N.; Wang, X.; Suchý, V.; Khan, I.; Zheng, X.; Liu, B.; Ardakani, O. H.; et al. Dispersed organic matter from pre-Devonian marine shales: A review on its composition, origin, evolution, and potential for hydrocarbon prospecting. *Earth-Sci. Rev.* **2025**, *261*, No. 105027.

(24) Peng, Q.; Du, B.; Xie, S.; Zheng, B. Organic Geochemistry and Oil-Source Correlation of Oil Seepages and Potential Source Rocks in Qiangtang Basin China. *ACS Omega* **2022**, *7* (34), 29612−29624.

(25) Al-Matary, A. M.; Hakimi, M. H.; Mustapha, K. A.; Rahim, A.; Naseem, W.; Al-Shawafi, Z. A. Molecular Compositions of Oil-Bearing Sandstones and Oil-Asphaltenes from the Kharir Oilfields in the Western Central Masila Basin Yemen. *ACS Omega* **2024**, *9* (15), 17398−17414.

(26) Radke, M.; Welte, D. H.; Willsch, H. Maturity parameters based on aromatic hydrocarbons: Influence of the organic matter type. *Org. Geochem.* **1986**, *10* (1), 51−63.

(27) Peters, K. E.; Walters, C. C.; Moldowan, J. M. *The Biomarker Guide: Vol. 2: Biomarkers and Isotopes in Petroleum Systems and Earth History*. 2 ed.; Cambridge University Press: Cambridge, 2005; *2*.

(28) Kvalheim, O. M.; Christy, A. A.; Telnæs, N.; Bjørseth, A. Maturity determination of organic matter in coals using the methylphenanthrene distribution. *Geochim. Cosmochim. Acta* **1987**, *51* (7), 1883−1888.

(29) Tissot, B. P.; Welte, D. H. *Petroleum Formation and Occurrence*; Springer: Berlin, Heidelberg, 1989.

(30) Radke, M.; Rullkötter, J.; Vriend, S. P. Distribution of naphthalenes in crude oils from the Java Sea: Source and maturation effects. *Geochim. Cosmochim. Acta* **1994**, *58* (17), 3675−3689.

(31) Wang, Q.; Huang, H.; Zheng, L. Thermal maturity parameters derived from tetra-, penta-substituted naphthalenes and organosulfur compounds in highly mature sediments. *Fuel* **2021**, *288*, No. 119626.

(32) Hegazi, A. H.; El-Gayar, M. S. Geochemical characterization of biodegraded crude oil, Assran Field, central Gulf of Suez. *J. Pet. Geol.* **2009**, *32* (4), 343−355.

(33) Thompson-Butler, W.; Peters, K. E.; Magoon, L. B.; Scheirer, A. H.; Moldowan, J. M.; Blanco, V. O.; Gonzalez, R. E.; Graham, S. A.; Zumberge, J. E.; Wavrek, D. A. Identification of genetically distinct petroleum tribes in the Middle Magdalena Valley Colombia. *AAPG Bull.* **2019**, *103* (12), 3003−3034.

(34) Xiao, H.; Li, M.; Nettersheim, B. J. Short chain tricyclic terpanes as organic proxies for paleo-depositional conditions. *Chem. Geol.* **2024**, *652*, No. 122023.

https://doi.org/10.1021/acsomega.4c08477
ACS Omega 2025, 10, 2735−2761

(35) Goodarzi, F. A climate change event, detected in Viséan oil shales from Devon Island Arctic Canada. *Int. J. Coal Geol.* **2020**, *226*, No. 103503.
(36) Qiao, J.; Luo, Q.; Guo, S.; Tang, X.; Kopaevich, L.; Littke, R. Organic petrology and geochemistry of the late Neogene Shizigou Formation in the Qaidam Basin, China: Characteristics of a prospective microbial gas source rock. *Int. J. Coal Geol.* **2024**, *296*, No. 104658.
(37) Qiao, J.; Baniasad, A.; Zieger, L.; Zhang, C.; Luo, Q.; Littke, R. Paleo-depositional environment, origin and characteristics of organic matter of the Triassic Chang 7 Member of the Yanchang Formation throughout the mid-western part of the Ordos Basi China n. *Int. J. Coal Geol.* **2021**, *237*, No. 103636.
(38) Zheng, T.; Zieger, L.; Baniasad, A.; Grohmann, S.; Hu, T.; Littke, R. The Shahejie Formation in the Dongpu Depression, Bohai Bay Basin, China: Geochemical investigation of the origin, deposition and preservation of organic matter in a saline lacustrine environment during the Middle Eocene. *Int. J. Coal Geol.* **2022**, *253*, No. 103967.
(39) Farrimond, P.; Taylor, A.; TelnÆs, N. Biomarker maturity parameters: the role of generation and thermal degradation. *Org. Geochem.* **1998**, *29* (5), 1181−1197.
(40) Sachse, V. F.; Littke, R.; Heim, S.; Kluth, O.; Schober, J.; Boutib, L.; Jabour, H.; Perssen, F.; Sindern, S. Petroleum source rocks of the Tarfaya Basin and adjacent areas Morocco. *Org. Geochem.* **2011**, *42* (3), 209−227.
(41) Liu, M.; Philp, R. P. Utilization of Pyrrolic Compounds as Indicators of Secondary Migration for Woodford Oils in the Anadarko Basin, Oklahoma, USA. *J. Earth Sci.* **2024**, *35* (5), 1499−1512.
(42) Riboulleau, A.; Schnyder, J.; Riquier, L.; Lefebvre, V.; Baudin, F.; Deconinck, J.-F. Environmental change during the Early Cretaceous in the Purbeck-type Durlston Bay section (Dorset, Southern England): A biomarker approach. *Org. Geochem.* **2007**, *38* (11), 1804−1823.
(43) Didyk, B. M.; Simoneit, B. R. T.; Brassell, S. C.; Eglinton, G. Organic geochemical indicators of palaeoenvironmental conditions of sedimentation. *Nature.* **1978**, *272* (5650), 216−222.
(44) Ma, X.; Wei, L.; Hou, D.; Xu, C.; Man, Y.; Li, W.; Wu, P. Geochemical Characteristics of Three Oil Families and Their Possible Source Rocks in the Sub-Sag A of Weixinan Depression, Beibuwan Basin Offshore South China Sea. *ACS Omega* **2022**, *7* (28), 24795−24811.
(45) Wu, Z.; Grohmann, S.; Littke, R. Geochemistry and petrology of Early Permian lacustrine shales in the Lodève Basin, Southern France: Depositional history, organic matter accumulation and thermal maturity. *Int. J. Coal Geol.* **2024**, *284*, No. 104469.
(46) Zhang, Q.; Grohmann, S.; Xu, X.; Littke, R. Depositional environment and thermal maturity of the coal-bearing Longtan Shale in southwest Guizhou, China: Implications for shale gas resource potential. *Int. J. Coal Geol.* **2020**, *231*, No. 103607.
(47) Lei, C.; Yin, S.; Ye, J.; Wu, J.; Wang, Z.; Gao, B. Geochemical Characteristics and Hydrocarbon Generation Modeling of the Paleocene Source Rocks in the Jiaojiang Sag, East China Sea Basin. *J. Earth Sci.* **2024**, *35* (2), 642−654.
(48) Romero-Viana, L.; Kienel, U.; Sachse, D. Lipid biomarker signatures in a hypersaline lake on Isabel Island (Eastern Pacific) as a proxy for past rainfall anomaly (1942−2006AD). *Paleogeogr. Paleoclimatol. Paleoecol.* **2012**, *350*−*352*, 49−61.
(49) Moldowan, J. M.; Seifert, W. K.; Gallegos, E. J. Relationship Between Petroleum Composition and Depositional Environment of Petroleum Source Rocks1. *AAPG Bull.* **1985**, *69* (8), 1255−1268.
(50) Asif, M.; Alexander, R.; Fazeelat, T.; Grice, K. Sedimentary processes for the geosynthesis of heterocyclic aromatic hydrocarbons and fluorenes by surface reactions. *Org. Geochem.* **2010**, *41* (5), 522−530.
(51) Pu, F.; Philip, R. P.; Zhenxi, L.; Guangguo, Y. Geochemical characteristics of aromatic hydrocarbons of crude oils and source rocks from different sedimentary environments. *Org. Geochem.* **1990**, *16* (1), 427−435.
(52) Fan, P.; Philp, R. P.; Li, Z.; Yu, X.; Ying, G. Biomarker distributions in crude oils and source rocks from different sedimentary environments. *Chem. Geol.* **1991**, *93* (1), 61−78.
(53) Volk, H.; George, S. C.; Middleton, H.; Schofield, S. Geochemical comparison of fluid inclusion and present-day oil accumulations in the Papuan Foreland−evidence for previously unrecognised petroleum source rocks. *Org. Geochem.* **2005**, *36* (1), 29−51.
(54) Hao, F.; Zhou, X.; Zhu, Y.; Yang, Y. Mechanisms for oil depletion and enrichment on the Shijiutuo uplift, Bohai Bay Basin China. *AAPG Bull.* **2009**, *93* (8), 1015−1037.
(55) Hao, F.; Zhou, X.; Zhu, Y.; Yang, Y. Lacustrine source rock deposition in response to co-evolution of environments and organisms controlled by tectonic subsidence and climate, Bohai Bay Basin China. *Org. Geochem.* **2011**, *42* (4), 323−339.
(56) Guo, R.; Zhao, Y.; Wang, W.; Hu, X.; Zhou, X.; Hao, L.; Ma, X.; Ma, D.; Li, S. Application of Rare-Earth Elements and Comparison to Molecular Markers in Oil−Source Correlation of Tight Oil: A Case Study of Chang 7 of the Upper Triassic Yanchang Formation in Longdong Area, Ordos Basin China. *ACS Omega* **2020**, *5* (35), 22140−22156.
(57) Liu, S.; Jiang, L.; Liu, B.; Zhao, C.; Tang, S.; Tan, F. Investigation of Organic Matter Sources and Depositional Environment Changes for Terrestrial Shale Succession from the Yuka Depression: Implications from Organic Geochemistry and Petrological Analyses. *J. Earth Sci.* **2023**, *34* (5), 1577−1595.
(58) Meyers, P. A. Organic geochemical proxies of paleoceanographic, paleolimnologic, and paleoclimatic processes. *Org. Geochem.* **1997**, *27* (5), 213−250.
(59) Sachse, D.; Sachs, J. P. Inverse relationship between D/H fractionation in cyanobacterial lipids and salinity in Christmas Island saline ponds. *Geochim. Cosmochim. Acta* **2008**, *72* (3), 793−806.
(60) Luo, Q.; George, S. C.; Xu, Y.; Zhong, N. Organic geochemical characteristics of the Mesoproterozoic Hongshuizhuang Formation from northern China: Implications for thermal maturity and biological sources. *Org. Geochem.* **2016**, *99*, 23−37.
(61) Ficken, K. J.; Li, B.; Swain, D. L.; Eglinton, G. An n-alkane proxy for the sedimentary input of submerged/floating freshwater aquatic macrophytes. *Org. Geochem.* **2000**, *31* (7), 745−749.
(62) Coetzee, J. A. *Pollen analytical studies in East and Southern Africa*; Palaeoecology of Africa, 1967.
(63) Nichols, J. E.; Booth, R. K.; Jackson, S. T.; Pendall, E. G.; Huang, Y. Paleohydrologic reconstruction based on n-alkane distributions in ombrotrophic peat. *Org. Geochem.* **2006**, *37* (11), 1505−1513.
(64) Bingham, F. M.; Foltz, G. R.; McPhaden, M. J. Seasonal cycles of surface layer salinity in the Pacific Ocean. *Ocean Sci.* **2010**, *6* (3), 775−787.
(65) Simoneit, B. R. T. Biomarkers (molecular fossils) as geochemical indicators of life. *Adv. Space Res.* **2004**, *33* (8), 1255−1261.
(66) Huang, W.-Y.; Meinschein, W. G. Sterols as ecological indicators. *Geochim. Cosmochim. Acta* **1979**, *43* (5), 739−745.
(67) Shao, M.; Lei, T.; Zhang, S.; Zhang, S.; Pei, Y.; Song, S. Effects of Volcanic Activity on Organic Matter Sources and the Paleoenvironment: Geochemical Evidence from Upper Carboniferous Source Rocks (Batamayineishan Formation) in Eastern Junggar NW China. *J. Earth Sci.* **2024**, *35* (5), 1482−1498.
(68) Summons, R. E.; Powell, T. G. Identification of aryl isoprenoids in source rocks and crude oils: Biological markers for the green sulphur bacteria. *Geochim. Cosmochim. Acta* **1987**, *51* (3), 557−566.
(69) Shiea, J.; Brassell, S. C.; Ward, D. M. Mid-chain branched mono- and dimethyl alkanes in hot spring cyanobacterial mats: A direct biogenic source for branched alkanes in ancient sediments? *Org. Geochem.* **1990**, *15* (3), 223−231.
(70) Sinninghe Damsté, J. S.; Kenig, F.; Koopmans, M. P.; Köster, J.; Schouten, S.; Hayes, J. M.; de Leeuw, J. W. Evidence for gammacerane as an indicator of water column stratification. *Geochim. Cosmochim. Acta* **1995**, *59* (9), 1895−1900.
(71) Kenig, F. C16−C29 homologous series of monomethylalkanes in the pyrolysis products of a Holocene microbial mat. *Org. Geochem.* **2000**, *31* (2), 237−241.
(72) Farrimond, P.; Talbot, H. M.; Watson, D. F.; Schulz, L. K.; Wilhelms, A. Methylhopanoids: Molecular indicators of ancient

https://doi.org/10.1021/acsomega.4c08477
ACS Omega 2025, 10, 2735−2761

bacteria and a petroleum correlation tool. *Geochim. Cosmochim. Acta* **2004**, *68* (19), 3873−3882.
(73) Bauersachs, T.; Schouten, S.; Compaoré, J.; Wollenzien, U.; Stal, L. J.; Damsté, J. S. S. Nitrogen Isotopic Fractionation Associated with Growth on Dinitrogen Gas and Nitrate by Cyanobacteria. *Limnol. Oceanogr.* **2009**, *54* (4), 1403−1411.
(74) Pawlowska, M. M.; Butterfield, N. J.; Brocks, J. J. Lipid taphonomy in the Proterozoic and the effect of microbial mats on biomarker preservation. *Geology* **2013**, *41* (2), 103−106.
(75) Philp, R. P.; Gilbert, T. D. Biomarker distributions in Australian oils predominantly derived from terrigenous source material. *Org. Geochem.* **1986**, *10* (1), 73−84.
(76) Peters, K. E.; Moldowan, J. M *The Biomarker Guide: Interpreting Molecular Fossils in Petroleum and Ancient Sediments*; Englewood Cliffs Nj Prentice Hall, 1992.
(77) Volkman, J. K.; Zhang, Z.; Xie, X.; Qin, J.; Borjigin, T. Biomarker evidence for Botryococcus and a methane cycle in the Eocene Huadian oil shale NE China. *Org. Geochem.* **2015**, *78*, 121−134.
(78) Xiao, H.; Li, M.; Wang, T.; You, B.; Lu, X.; Wang, X. Organic molecular evidence in the∼ 1.40 Ga Xiamaling Formation black shales in North China Craton for biological diversity and paleoenvironment of mid-Proterozoic ocean. *Precambrian Res.* **2022**, *381*, No. 106848.
(79) Hassan, M.; Leila, M. L.; Ahmed, M.; Issa, G.; Šegvić, B.; Hegab, O. Hydrocarbon-Source Correlation in the Obayied Sub-Basin, North Western Desert, Egypt: Controls on Generation of Natural Gas and Light Crude Hydrocarbon Blends. *J. Earth Sci.* **2024**, *35* (6), 1944−1965.
(80) Volkman, J. Sterols in microorganisms. *Appl. Microbiol. Biotechnol.* **2003**, *60* (5), 495−506.
(81) Ourisson, G.; Rohmer, M. Hopanoids. 2. Biohopanoids: a novel class of bacterial lipids. *Acc. Chem. Res.* **1992**, *25* (9), 403−408.
(82) Rohrssen, M.; Love, G. D.; Fischer, W.; Finnegan, S.; Fike, D. A. Lipid biomarkers record fundamental changes in the microbial community structure of tropical seas during the Late Ordovician Hirnantian glaciation. *Geology* **2013**, *41* (2), 127−130.
(83) Strachan, R. A.; May, F.; Barr, D., The Glenfinnan and Loch Eil Divisions of the Moine Assemblage. In *Later Proterozoic Stratigraphy of the Northern Atlantic Regions*, Winchester, J. A., Ed.; Springer US: Boston, MA, 1988; 32−45.
(84) Ellis, L.; Singh, R. K.; Alexander, R.; Kagi, R. I. Formation of isohexyl alkylaromatic hydrocarbons from aromatization-rearrangement of terpenoids in the sedimentary environment: A new class of biomarker. *Geochim. Cosmochim. Acta* **1996**, *60* (23), 4747−4763.
(85) Armstroff, A.; Wilkes, H.; Schwarzbauer, J.; Littke, R.; Horsfield, B. Aromatic hydrocarbon biomarkers in terrestrial organic matter of Devonian to Permian age. *Paleogeogr. Paleoclimatol. Paleoecol.* **2006**, *240* (1), 253−274.
(86) Grice, K.; Audino, M.; Boreham, C. J.; Alexander, R.; Kagi, R. I. Distributions and stable carbon isotopic compositions of biomarkers in torbanites from different palaeogeographical locations. *Org. Geochem.* **2001**, *32* (10), 1195−1210.
(87) Budzinski, H.; Garrigues, P.; Connan, J.; Devillers, J.; Domine, D.; Radke, M.; Oudins, J. L. Alkylated phenanthrene distributions as maturity and origin indicators in crude oils and rock extracts. *Geochim. Cosmochim. Acta* **1995**, *59* (10), 2043−2056.
(88) van Aarssen, B. G. K.; Alexander, R.; Kagi, R. I. Higher plant biomarkers reflect palaeovegetation changes during Jurassic times. *Geochim. Cosmochim. Acta* **2000**, *64* (8), 1417−1424.
(89) Grice, K.; Cao, C.; Love, G. D.; Böttcher, M. E.; Twitchett, R. J.; Grosjean, E.; Summons, R. E.; Turgeon, S. C.; Dunning, W.; Jin, Y. Photic Zone Euxinia During the Permian-Triassic Superanoxic Event. *Science* **2005**, *307* (5710), 706−709.
(90) Chaffee, A. L.; Johns, R. B. Polycyclic aromatic hydrocarbons in Australian coals. I. Angularly fused pentacyclic tri- and tetraaromatic components of Victorian brown coal. *Geochim. Cosmochim. Acta* **1983**, *47* (12), 2141−2155.
(91) Chaffee, A. L.; Fookes, C. J. R. Polycyclic aromatic hydrocarbons in Australian coals—III. Structural elucidation by proton nuclear magnetic resonance spectroscopy. *Org. Geochem.* **1988**, *12* (3), 261−271.
(92) Otto, A.; Wilde, V. Sesqui-, di-, and triterpenoids as chemosystematic markers in extant conifers—A review. *Bot. Rev.* **2001**, *67* (2), 141−238.
(93) Haberer, R. M.; Mangelsdorf, K.; Wilkes, H.; Horsfield, B. Occurrence and palaeoenvironmental significance of aromatic hydrocarbon biomarkers in Oligocene sediments from the Mallik 5L-38 Gas Hydrate Production Research Well (Canada). *Org. Geochem.* **2006**, *37* (5), 519−538.
(94) Romero-Sarmiento, M.-F.; Riboulleau, A.; Vecoli, M.; Versteegh, G. J. M. Aliphatic and aromatic biomarkers from Gondwanan sediments of Late Ordovician to Early Devonian age: An early terrestrialization approach. *Org. Geochem.* **2011**, *42* (6), 605−617.
(95) Huang, H.; Zhang, S.; Su, J. Pyrolytically Derived Polycyclic Aromatic Hydrocarbons in Marine Oils from the Tarim Basin NW China. *Energy Fuels.* **2015**, *29* (9), 5578−5586.
(96) Sofer, Z. Stable Carbon Isotope Compositions of Crude Oils: Application to Source Depositional Environments and Petroleum Alteration1. *AAPG Bull.* **1984**, *68* (1), 31−49.
(97) Collister, J. W.; Wavrek, D. A. δ13C compositions of saturate and aromatic fractions of lacustrine oils and bitumens: evidence for water column stratification. *Org. Geochem.* **1996**, *24* (8), 913−920.
(98) Qiao, J.; Liu, L.; Shang, X. Deposition conditions of the Jurassic lacustrine source rocks in the East Fukang Sag, Junggar Basin, NW China: Evidence from major and trace elements. *Geol. J.* **2020**, *55* (7), 4936−4953.
(99) Blumer, M.; Ehrhardt, M.; Jones, J. H. The environmental fate of stranded crude oil. *Deep Sea Res.* **1973**, *20* (3), 239−259.
(100) Chen, G.; Wang, D.; Yang, F.; Tang, Y.; Zou, X.; Ma, W.; Li, M. Organic geochemistry and controlling factors of alkaline source rocks within sequence stratigraphic framework in the Fengcheng Formation, Mahu sag, Junggar Basin NW China. *Energy Explor. Exploit.* **2022**, *40* (3), 1057−1077.
(101) Liu, S.; Gao, G.; Gang, W.; Xiang, B.; Wang, M.; Wang, C. Comparison of Formation Conditions of Source Rocks of Fengcheng and Lucaogou Formations in the Junggar Basin, NW China: Implications for Organic Matter Enrichment and Hydrocarbon Potential. *J. Earth Sci.* **2023**, *34* (4), 1026−1040.
(102) Yu, S.; Wang, X.; Xiang, B.; Ren, J.; Li, E.; Wang, J.; Huang, P.; Wang, G.; Xu, H.; Pan, C. Molecular and carbon isotopic geochemistry of crude oils and extracts from Permian source rocks in the northwestern and central Junggar Basin China. *Org. Geochem.* **2017**, *113*, 27−42.
(103) Ding, X.; Qu, J.; Imin, A.; Zha, M.; Su, Y.; Jiang, Z.; Jiang, H. Organic matter origin and accumulation in tuffaceous shale of the lower Permian Lucaogou Formation Jimsar Sag. *J. Pet. Sci. Eng.* **2019**, *179*, 696−706.
(104) Feng, C.; Li, T.; He, W.; Zheng, M. Organic geochemical traits and paleo-depositional conditions of source rocks from the Carboniferous to Permian sediments of the northern Mahu Sag, Junggar Basin China. *J. Pet. Sci. Eng.* **2020**, *191*, No. 107117.
(105) Feng, C.; He, W.; Cai, H.; Zhang, J.; Nie, Y. Organic geochemical characteristics and comparison of the source rocks and the severely biodegradable oil sands around Karamay China. *Energy Explor. Exploit.* **2021**, *39* (1), 108−133.
(106) Wang, Y.; Cao, J.; Tao, K.; Li, E.; Ma, C.; Shi, C. Reevaluating the source and accumulation of tight oil in the middle Permian Lucaogou Formation of the Junggar Basin China. *Mar. Pet. Geol.* **2020**, *117*, No. 104384.
(107) Wang, T.; Cao, J.; Jin, J.; Xia, L.; Xiang, B.; Ma, W.; Li, W.; He, W. Spatiotemporal evolution of a Late Paleozoic alkaline lake in the Junggar Basin China. *Mar. Pet. Geol.* **2021**, *124*, No. 104799.
(108) Xia, L.; Cao, J.; Lee, C.; Stüeken, E. E.; Zhi, D.; Love, G. D. A new constraint on the antiquity of ancient haloalkaliphilic green algae that flourished in a ca. 300 Ma Paleozoic lake. *Geobiology* **2021**, *19* (2), 147−161.
(109) Liu, Y.; Zeng, J.; Jin, J.; Yang, G.; Xiang, B.; Zhou, N.; Ma, W.; Qiao, J.; Li, S.; Liu, S. Geochemical evaluation of produced petroleum

https://doi.org/10.1021/acsomega.4c08477
ACS Omega 2025, 10, 2735−2761

from the Middle Permian Lucaogou reservoirs Junggar Basin and its implication for the unconventional shale oil play. *J. Pet. Sci. Eng.* **2022**, *211*, No. 110202.
(110) Liu, S.; Gao, G.; Jin, J.; Gang, W.; Xiang, B. Source rock with high abundance of C28 regular sterane in typical brackish-saline lacustrine sediments: Biogenic source, depositional environment and hydrocarbon generation potential in Junggar Basin China. *J. Pet. Sci. Eng.* **2022**, *208*, No. 109670.
(111) Wang, Y.; Cao, J.; Tao, K.; Xiao, W.; Xiang, B.; Li, E.; Pan, C. Absence of β-carotane as proxies of hydrothermal activity in brackish lacustrine sediments. *Paleogeogr. Paleoclimatol. Paleoecol.* **2022**, *587*, No. 110801.
(112) Ding, X.-J.; He, W.-J.; Liu, H.-L.; Guo, X.-G.; Zha, M.; Jiang, Z.-F. Organic matter accumulation in lacustrine shale of the Permian Jimsar Sag, Junggar Basin NW China. *Pet. Sci.* **2023**, *20* (3), 1327−1346.
(113) Zeng, W.; Zhang, Z.; Wang, B.; Chen, X.; Zheng, R.; Fu, G.; Jin, Y. Formation mechanism of organic-rich mixed sedimentary rocks in saline lacustrine basin, Permian Lucaogou Formation, Jimsar Sag, Junggar Basin Northwest China. *Mar. Pet. Geol.* **2023**, *156*, No. 106452.
(114) Zhi, D.; Xiang, B.; Zhou, N.; Li, E.; Zhang, C.; Wang, Y.; Cao, J. Contrasting shale oil accumulation in the upper and lower sweet spots of the lacustrine Permian Lucaogou Formation, Junggar Basin China. *Mar. Pet. Geol.* **2023**, *150*, No. 106178.

https://doi.org/10.1021/acsomega.4c08477
ACS Omega 2025, 10, 2735−2761